Journal of Colloid and Interface Science 627 (2022) 283–298

Contents lists available at ScienceDirect

Journal of Colloid and Interface Science

journal homepage: www.elsevier.com/locate/jcis

Transport of cationic liposomes in a human blood brain barrier model: Role of the stereochemistry of the gemini amphiphile on liposome biological features

Beatrice Simonis [a,b,1], Domenico Vignone [c,1], Odalys Gonzalez Paz [c], Enrica Donati [d], Maria Laura Falchetti [e], Cecilia Bombelli [b], Antonella Cellucci [c], Giulio Auciello [c], Ivan Fini [c], Luciano Galantini [a], Rudaba Zaman Syeda [a], Marco Mazzonna [d], Maria Patrizia Mongiardi [e], Francesco Buonocore [f], Francesca Ceccacci [b,*], Annalise Di Marco [c,**], Giovanna Mancini [d]

[a] Sapienza Università di Roma, Dipartimento di Chimica, P.le A. Moro 5, Rome, Italy
[b] CNR-ISB, Istituto per i Sistemi Biologici, Sede Secondaria di Roma-Meccanismi di Reazione c/o Dipartimento di Chimica, Sapienza Università di Roma, P.le A. Moro 5, Rome, Italy
[c] IRBM SpA, via Pontina Km 30.600, 00071 Pomezia (Rome), Italy
[d] CNR-ISB, Istituto per i Sistemi Biologici, Area della Ricerca di Roma 1, Strada Provinciale 35d 9, 00020 Montelibretti, Rome, Italy
[e] CNR-IBBC, Istituto di Biochimica e Biologia Cellulare, Via E. Ramarini, 32, 00015 MonterotondoScalo, Rome, Italy
[f] Dipartimento per la Innovazione nei sistemi biologici, agroalimentari e forestali, Università della Tuscia (DIBAF), Largo dell'Università snc, 01100 Viterbo, Italy

GRAPHICAL ABSTRACT

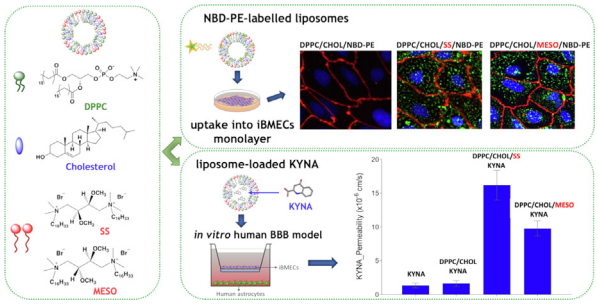

ARTICLE INFO

Article history:
Received 11 February 2022
Revised 6 June 2022
Accepted 4 July 2022
Available online 6 July 2022

ABSTRACT

Hypothesis: The positive charge on liposome surface is known to promote the crossing of the Blood brain barrier (BBB). However, when diastereomeric cationic gemini amphiphiles are among lipid membrane components, also the stereochemistry may affect the permeability of the vesicle across the BBB.
Experiments: Liposomes featuring cationic diasteromeric gemini amphiphiles were formulated, characterized, and their interaction with cell culture models of BBB investigated.

Abbreviations: hiPSC, human induced pluripotent stem cells; CNS, central nervous system; BBB, blood brain barrier; BCECs, brain capillaries endothelial cells; LDL, low-density lipoprotein; TAT, trans-activating transcriptor; CPP, cell-penetrating peptide; hiPSC-derived BMECs or iBMECs, brain microvascular endothelial cells derived from human induced pluripotent stem cells; KYNA, kynurenic acid; PDI, polydispersity index; T_m, transition temperature; CHOL, cholesterol; DLS, dynamic laser light scattering; HUVEC, Human Umbilical Vein Endothelial Cells; PM, plasma membrane; mPEG-DSPE, 1,2-distearoyl-*sn*-glycero-3-phosphoethanolamine-N[methoxy(polyethyleneglycol) 2000] (ammonium salt); DPPC, 1,2-dipalmitoyl-*sn*-glycero-3-phosphocholine; PA-PEG3-mannose, 1,2-dipalmitoyl-*sn*-glycero-3-phospho(ethyl-1′,1′,3′-triazole)triethylene glycolmannose) (ammonium salt, 16:0); POPC, 1-palmitoyl-2-oleoyl-*sn*-glycero-3-phosphocholine; NBD-PE 16:0, 1,2-dipalmitoyl-*sn*-glycero-3-phosphoethanolamine-N-((7-nitro-2-1.3-benzoxadiazol-4-yl) ammonium salt; Rhod-PE 16:0, 1,2-dipalmitoyl-*sn*-glycero-3-phosphoethanolamine-N-(lissamine rhodamine B sulfonyl) ammonium salt.

* Corresponding authors at: CNR-Institute for Biological Systems (ISB) secondary office of Rome-Reaction Mechanisms c/o Department of Chemistry, Sapienza University, P. le A. Moro 5, 00185 Roma Italy.
** Corresponding authors at: High content Biology and Screening, IRBM SpA, via Pontina Km 30.6, 00071 Pomezia, RM, Italy
E-mail addresses: francesca.ceccacci@cnr.it (F. Ceccacci), A.DiMarco@irbm.com (A. Di Marco).
[1] The authors contributed equally to the work.

https://doi.org/10.1016/j.jcis.2022.07.025

Keywords:
Blood brain barrier
Liposome
Drug delivery
Permeability
Transport model
Brain monolayer endothelial cell
Gemini amphiphile
Stereochemistry

Findings: Liposomes featuring the gemini amphiphiles were internalized in a monolayer of brain microvascular endothelial cells derived from human induced pluripotent stem cells (hiPSC) through an energy dependent transport, internalization involving both clathrin- and caveolae-mediated endocytosis. On the same formulations, the permeability was also evaluated across a human derived *in vitro* BBB transport model. The permeability of liposomes featuring the gemini amphiphiles was significantly higher compared to that of neutral liposomes (DPPC/Cholesterol), that were not able to cross BBB. Most importantly, the permeability was influenced by the stereochemistry of the gemini and pegylation of these formulations did not result in a drastic reduction of the crossing ability.

The *in vitro* iPSC-derived BBB models used in this work represent an important advancement in the drug discovery research of novel brain delivery strategies and therapeutics for central nervous system diseases.

1. Introduction

Nearly 1 billion people of the world's population suffers from diseases of the central nervous system (CNS) and, with the ageing of global population, neurological disorders have become one of the greatest medical emergencies. Despite the efforts to implement novel therapeutic approaches, the development of new drugs for the CNS is severely hampered by the presence of the blood brain barrier (BBB) which prevents almost the totality of the drug candidates from reaching the CNS at a therapeutic concentration [1–3].

Among the most selective barriers in the human organism, the BBB is a dynamic and complex interface between blood and CNS and plays a crucial role in controlling the efflux and influx of substances. Its complex organization is responsible for peculiar features such as limited paracellular and *trans*-cellular permeability and transport.[4–7] Thanks to these characteristics, the BBB is able to protect the brain against external aggressions by regulating molecular transport and elimination of waste product, while allowing nutrients to reach neurons.[5,6,8] However, this impressive control does not allow therapeutics to reach targets in the brain (>98 % of low-molecular-weight drugs and almost all large therapeutics do not cross the BBB).[5] Some procedures for direct drug administration into brain have been explored, such as cerebrospinal fluid or intranasal delivery, but these techniques are invasive and/or often scarcely effective.[9].

For these reasons, since drug delivery rather than drug efficacy is the crucial issue in the treatment of CNS diseases, there is an urgent need to develop suitable vectors to enable drug delivery through the BBB.

In this context, nanosystems such as liposomes may represent the ideal candidates because, due to their nature, they offer several advantages including biocompatibility, biodegradability, low potential for toxicity and immunogenicity, ease of preparation, the ability to encapsulate a wide range of drugs (both hydrophilic and hydrophobic ones) and, above all, the possibility of finely tuning their properties by modulating their composition and process of preparation.[10–16] For these reasons, liposomes are probably the most studied and investigated nanocarriers for targeted drug delivery.[17–22] To reach the CNS, liposomes need to be functionalized with targeting moieties able to trigger one among the different trans-cellular mechanisms involved in BBB crossing.[23,24] Decorating liposome surface with specific active ligands such as antibodies, transferrin, lactoferrin, low-density lipoprotein (LDL), insulin or glutathione, facilitates their binding to BBB and promotes receptor-mediated transcytosis.[23,25–31] The functionalization with sugar moieties represents another possible strategy, as transporters of glucose (SLC2A family) are widely expressed on brain capillaries endothelial cells (BCECs), especially SLC2A1 (GLUT1).[32] It has been reported that the presence of mannose residues on liposome's surface allows BBB crossing mediated by transporter.[33] In general, it is well known that the presence of a positive charge promotes the interaction of nanocarriers with the cell membrane, enhances uptake and increases the effective delivery of drugs, therapeutic and genes.[34–38] A cationic surface of liposomes should favour the crossing of BBB via non-specific mechanisms of *absorptive-mediated transcytosis*. It has already been shown that the functionalization of liposomes with trans-activating transcriptor (TAT), a short positively charged cell-penetrating peptide (CPP)[39], promotes the interaction with negatively charged BBB, triggering the penetration of the nanocarrier through BCECs.[40–42]

In this work we investigated the ability of cationic liposomes composed of a phosphocholine (DPPC), cholesterol and a cationic gemini amphiphile (SS, MESO or RR, Chart 1) to cross the BBB. In addition, we investigated the effect of the concurrent presence of both a cationic gemini amphiphile and a mannosylated lipid (PA-PEG3-PE-mannose, *i.e.* a lipid bearing a ligand able to bind GLUT1 transporter, Chart 1) on the features of liposome in the biological environment. Specifically, we investigated the interaction of liposomes with a monolayer of differentiated brain microvascular endothelial cells derived from human induced pluripotent stem cells (hiPSC-derived BMECs or iBMECs). The transport of selected liposome formulations was also evaluated across an *in vitro* BBB model established in transwell systems, made of iBMECs in co-culture with human astrocytes [43].

Previous investigations showed that the stereochemistry of gemini (SS and MESO) affects the physicochemical and biological features of diverse liposomes, both empty and loaded with different active principles, such as *m*-THPC (the active principle of Foscan)[44–46], DNA (calf thymus and plasmidic)[36,47] and siRNA.[48–50] In particular, gemini stereochemistry affects liposome size, ζ-potential, lipid bilayer organization, and stability; as a result, these differences, in turn, affect the delivery efficiency and intracellular fate of carrier and cargo in many cell types.[51–56] More generally, it has already been reported how the chirality of nanoparticles can affect biological responses [57].

The different behaviour of liposomes depending on gemini stereochemistry has been demonstrated in several experiments, in different cell models. What has never been studied is the ability of these formulations to cross BBB and the effect of gemini stereochemistry on the permeability of liposomes.

Liposome formulations were characterized in terms of size, polidispersity, and stability. Those showing appropriate size and stability were then evaluated both on iBMECs in monolayer and on the *in vitro* iBMECs model. The toxic potential of these formulations in primary human fibroblasts and endothelial cells, as well as haemolytic activity, was also evaluated.

2. Results and discussion

2.1. Characterization of liposomes

2.1.1. Preparation of liposomes

Different liposomes were formulated, composed of a saturated phospholipid (DPPC), cholesterol (CHOL), one of the cationic gemini amphiphiles (SS, MESO or RR, **Chart 1**), and/or a mannosylated phospholipid (PA-PEG3-mannose). Formulations including SS amphiphile were prepared also in the presence of a pegylated phospholipid (mPEG-DSPE).

The inclusion of cholesterol in the mixture enhances the stability of the lipid bilayer and gives it the so-called *bilayer-tightening effect,* inducing a dense packing and increasing the orientation order of lipid chains. This leads to a more compact structure with reduced permeability to water-soluble molecules and increased retention of the entrapped drug.[58,59]

In the formulation including SS gemini, mPEG-DSPE was also added to compare non-PEGylated and PEGylated formulations in terms of drug uptake and retention, stability over time, ability to bind with specific tissues or cells[23] and permeability across the BBB model. Indeed, the presence of PEG-conjugated lipids improves the stability of liposome in biological fluids by providing a protective hydrophilic film on liposome surface and hindering the interaction with plasma proteins.[60] It has also been reported that decorating liposome surface with PEG not only increases liposome-circulation life but also affects the uptake by target cells.[61–65]

The presence of a cationic amphiphile (SS, RR or MESO gemini) in the lipid bilayer should favour, as previously observed in the case of other cellular types [42,45], the electrostatic interaction with the negatively charged cell membranes of BBB epithelium, promoting the crossing *via absorptive-mediated transcytosis*. On the other hand, the inclusion of a mannosylated phospholipid (PA-PEG3-mannose) in the lipid bilayer should promote the crossing of BBB by *carrier-mediated endocytosis* (in the specific case Glut1) [33].

Liposomes were labelled with a fluorescent lipid for cytotoxicity experiments and for experiments on monolayer of brain tissue cultures (Rhod-PE 16:10 and NBD-PE 16:10, see next paragraphs). In the case of permeability experiments on the *in vitro* BBB model, liposomes were loaded with kynurenic acid (KYNA, Chart 1) that was used as a tracer.

Liposomes were prepared by the lipid film hydration method combined with the extrusion procedure and the freeze–thaw protocol in order to reduce their lamellarity and size, thus obtaining unilamellar vesicles of suitable dimensions (100–200 nm).

For all liposomes the mean diameter, the polydispersity index (PDI) and the transition temperature (T_m) were investigated. In addition, for KYNA-loaded liposomes, the content and release of entrapped KYNA in the final liposome suspensions were evaluated.

The most stable formulations selected for biological experiments are reported in Table 1 and 2. The ratios of lipid components were chosen as the result of a systematic investigation addressed to achieve liposomes of suitable dimension, stable to aggregation phenomena and capable of entrapping and retaining KYNA for the time necessary for biological permeability experiments.

Importantly, formulations containing amphiphile RR were not able to retain KYNA for the time required for biological experiments. Different conditions were explored, changing the ratio of lipid components and using POPC or DMPC instead of DPPC, but in all cases KYNA was soon released from RR-based liposomes.

Different lipid ratios were explored also in the case of liposomes formulated with PA-PEG3-mannose, in this case liposomes of suitable dimensions and capable of encapsulating KYNA for a sufficient time were obtained by including the SS amphiphile in the lipid bilayer (**F5a**, **F5b**, Table 1 and 2).

Table 1
Features of liposome formulations selected for biological experiments (10 mM total lipids) in HBSS –HEPES buffer (pH 7.4).

Formulation	Composition (mM)	Diameter (nm)	PdI	ζ-Potential (mV)
F1a	DPPC /CHOL 8.0: 2.0	140 ± 2	0.08 ± 0.02	7.9 ± 0.5
F2a	DPPC / CHOL / SS 5.6: 2.0: 2.4	159 ± 2	0.05 ± 0.03	35.2 ± 2.3
F3a	DPPC / CHOL / SS / mPEG-DSPE 5.6: 2.0: 2.4: 0.4	180 ± 3	0.10 ± 0.04	24.1 ± 1.3
F4a	DPPC / CHOL / MESO 5.6: 2.0: 2.4	143 ± 2	0.05 ± 0.02	33.8 ± 3.4
F5a	DPPC / CHOL / PA-PEG3-mannose / SS 5.6: 2.8: 0.2: 1.4	135 ± 1	0.10 ± 0.01	28.4 ± 1.4

Table 2
Features of liposome formulations selected for biological experiments (10 mM total lipids) in HBSS –HEPES buffer (pH 7.4). Formulations were hydrated with a 1 mM KYNA solution in HBSS–HEPES buffer (pH 7.4).

Formulation	Composition (mM)	Diameter (nm)	PdI	ζ-Potential (mV)	KYNA (μM)
F1b	DPPC / CHOL 8.0: 2.0	137 ± 1	0.10 ± 0.01	4.0 ± 1.7	19 ± 2
F2b	DPPC / CHOL / SS 5.6: 2.0: 2.4	160 ± 2	0.01 ± 0.03	32.5 ± 1.1	56 ± 3
F3b	DPPC / CHOL / SS / mPEG-DSPE 5.6: 2.0: 2.4: 0.4	183 ± 2	0.08 ± 0.03	26.1 ± 0.7	50 ± 2
F4b	DPPC / CHOL / MESO 5.6: 2.0: 2.4	147 ± 1	0.07 ± 0.02	23.2 ± 0.3	53 ± 3
F5b	DPPC / CHOL / PA-PEG3-mannose / SS 5.6: 2.8: 0.2: 1.4	118 ± 2	0.10 ± 0.01	27.2 ± 3.3	24 ± 4

2.1.2. Characterization of empty liposomes

Liposome particle size distribution and polydispersity index (PDI) as well as T_m were investigated by dynamic laser light scattering (DLS).

Empty liposomes **F1a-F5a** (Table 1) were monitored daily for 14 days to evaluate their stability over time in terms of aggregation phenomena, a crucial issue for biological investigations.

Results of DLS measurements show a narrow size distribution for all liposomes with a diameter of ~ 130–180 nm. **F1a-F5a** formulations were stable for seven days, after this period **F2a** (DPPC/CHOL/SS) formulation showed an increase in size due to vesicle aggregation whereas PEG-decorated **F3a** (DPPC/CHOL/SS/mPEG-DSPE) showed no tendency to aggregate. As expected, the presence of PEG-lipids in liposomes reduces surface-surface interaction, thus preventing aggregation.[66–68].

It is worth of note that **F4a** (DPPC/CHOL/MESO) formulation, containing the MESO amphiphile, remained substantially stable after 2 weeks.

The strong control of the stereochemistry of gemini on the organization of lipid bilayers, and hence on their morphology and physicochemical features, was not unexpected.[48,52,55,69,70] Actually, in previous studies it was shown that the different stereochemistry of SS and MESO gemini controls water exposure of hydrophilic groups, chain packing, interface curvature, and the morphology of the aggregates.[55,71].

The behaviour of **F1a-F5a** formulations as a function of temperature was studied to evaluate liposome transition temperature by monitoring scattering intensity and vesicles size by DLS. Generally, by increasing the temperature, formulations are expected to show an abrupt increase of the derived count rate at the transition. As the size of the aggregates does not show usually the same rise, the intensity jump is mainly ascribed to a change in the lipid bilayer refractive index, and hence to a change of its fluidity. In our case, a well recognizable transition was shown by **F1a** (DPPC/CHOL) formulation (T_m ~ 40°). However, the presence of a gemini component and its stereochemistry affected the behaviour

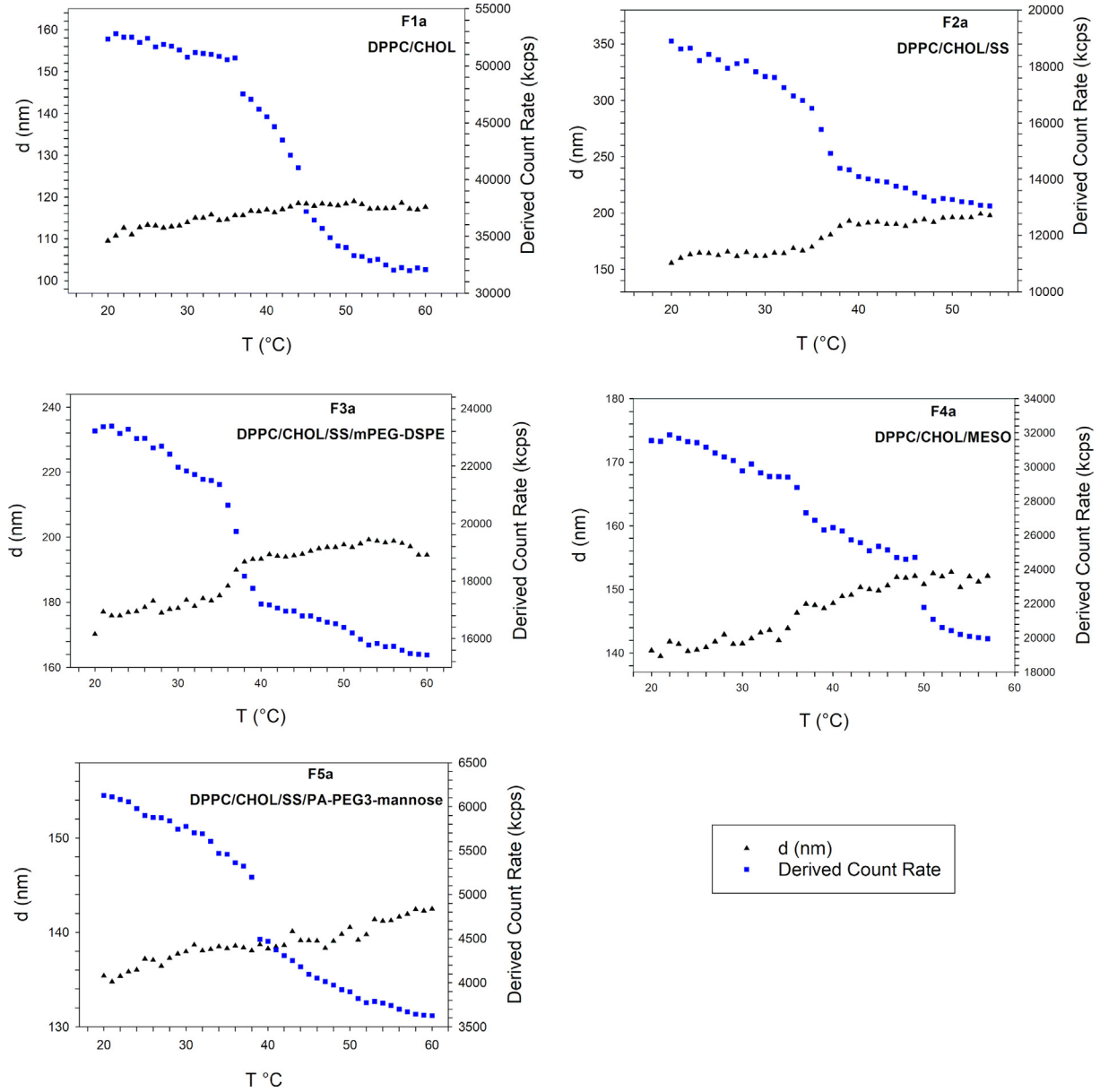

Fig. 1. Scattering Intensity (Derived Count Rate, blue square) and aggregate diameter (d, black triangle) measured as a function of temperature for formulations **F1a-F5a**. (For interpretation of the references to colour in this figure legend, the reader is referred to the web version of this article.)

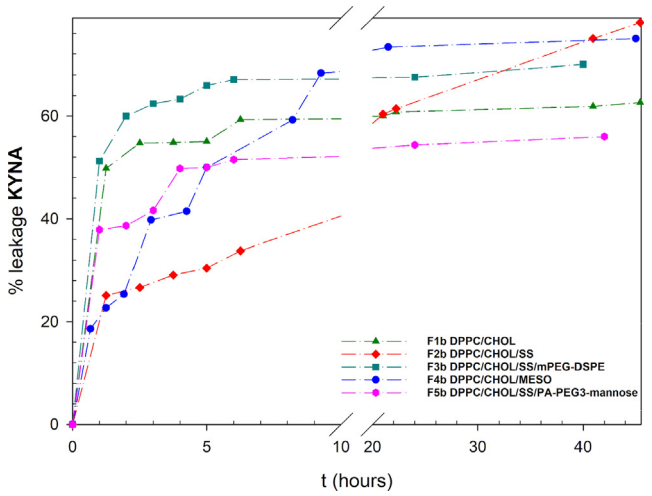

Fig. 2. Leakage of KYNA over time in the case of liposomes **F1b** (green triangle), **F2b** (red rhombus), **F3b** (green square), **F4b** (blue circle) and **F5b** (pink hexagon). The value is expressed as percentage of KYNA released with respect to initial KYNA concentration in liposomes. (For interpretation of the references to colour in this figure legend, the reader is referred to the web version of this article.)

of the formulations with respect to DPPC/CHOL liposomes. In the case of formulations **F2a** (DPPC/CHOL/SS) and **F3a** (DPPC/CHOL/SS/mPEG-DSPE), the presence of **SS** led to a less pronounced jump and to a decrease of T_m (~36 °C and 37 °C, respectively). This result suggests that in the case of **F2a** formulation the presence of SS smoothes the difference between the gel and the liquid-crystalline phase, likely due to the perturbation of the gel phase that becomes more fluid. In addition, the transition occurred in a short temperature range, indicating that it is cooperative and thus that SS has a good miscibility with the lipid bilayer. In the case of **F4a** (DPPC/CHOL/MESO), a clear transition was not detectable, as it occurred gradually in a wide temperature range, evidencing that MESO isomer is less miscible with the other lipid components than SS. The different effect of the two gemini on the T_m was already reported for other formulations.[53]

In the **F5a** formulation the presence of gemini SS and PA-PEG3-mannose induced a slight increase of the derived count rate at the transition temperature ($T_m \sim 38°$ C).

2.1.3. Characterization of KYNA-loaded liposomes

Based on the results obtained in the case of **F1a-F5a** empty liposomes, their capability to entrap and retain KYNA was investigated.

KYNA was entrapped by passive loading, using 1 mM KYNA in HBSS–HEPES solution to hydrate lipid films and obtain a final 10 mM total lipid concentration (Table 2, F1b-F5b). Removal of unentrapped KYNA was performed by size exclusion chromatography.

KYNA and lipid concentrations were chosen on the basis of preliminary experiments showing that higher KYNA concentrations or higher KYNA/lipid ratios lead to the formation of large and polydisperse aggregates.

F1b-F5b formulations, all containing KYNA, were characterized by monomodal distribution with a diameter in agreement with that imposed by the extrusion and an appropriate PDI (Table 2).

The loaded KYNA content (Table 2) was evaluated by HPLC measurements. The amount of CHOL was also determined in order to estimate lipid concentration after filtration by size exclusion chromatography.

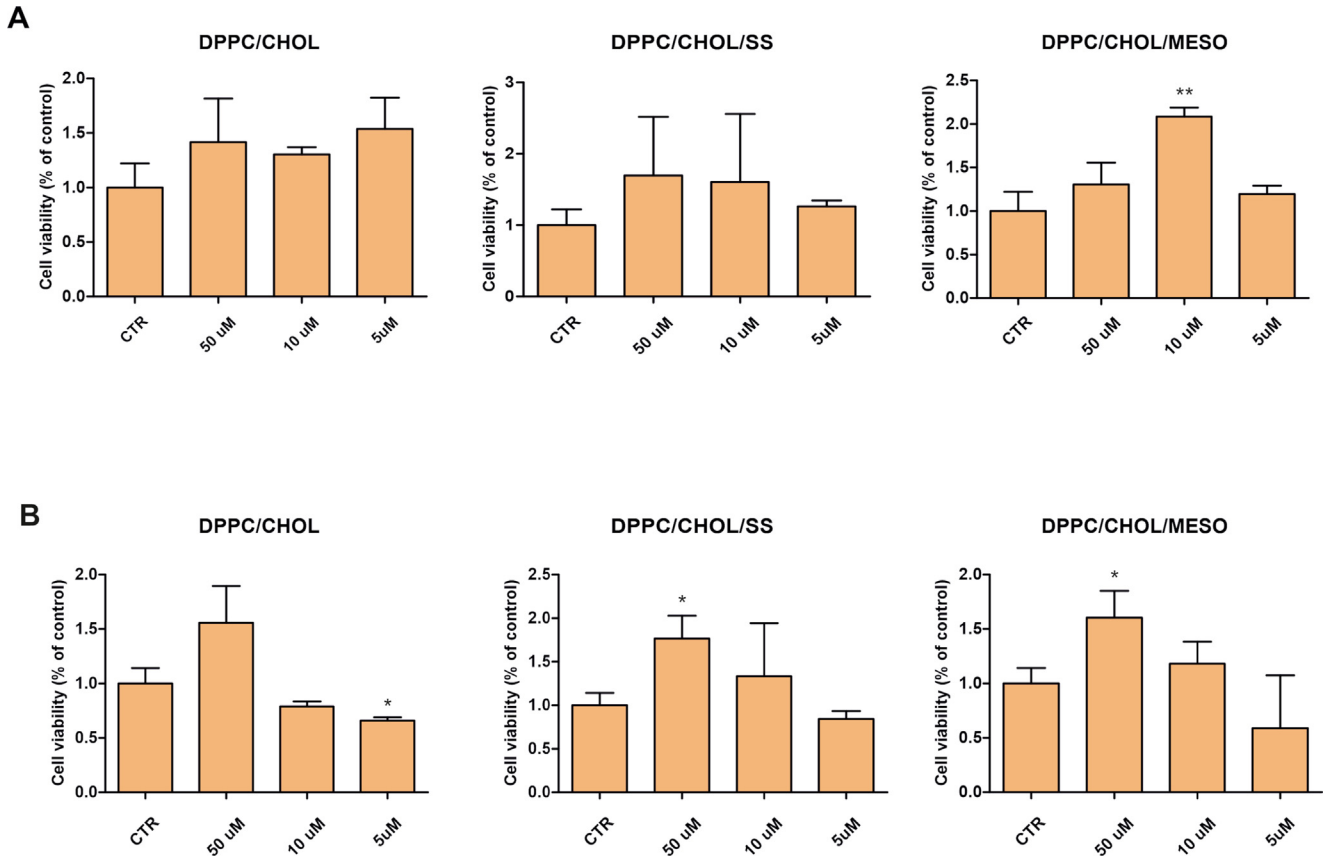

Fig. 3. Cell viability assay of BJ cells exposed to liposomes. Cells were exposed to liposomes for 6 h and cell viability was addressed by MTS assay 24 (A) and 48 h (B) following liposome withdrawal. n = 3 biological replicates. *p value < 0.05; **p value < 0.01.

Knowing the relatively low efficiency of passive loading method, initial concentration conditions were properly set to have a final encapsulated KYNA concentration suitable for biological experiments.

HPLC results showed that liposomes containing gemini amphiphiles (**F2b-F4b**) entrapped a higher amount of KYNA compared with liposomes formulated in the absence of gemini, *i.e.* DPPC/CHOL (**F1b**).

The leakage over time of KYNA from liposomes was monitored over a period of 24 h. A leakage of ~ 50 % was observed in all cases after 8–9 h (Fig. 2). However, the presence of gemini (**F2b, F4b, F5b**) resulted in a slower release with respect to **F1b** (DPPC/CHOL) formulation over the first 6 h after preparation.

Based on these results, the formulations were used for biological experiments immediately after the preparation, in order to have a suitable concentration of entrapped KYNA in all liposomes.

2.2. Experiments on human fibroblasts and primary endothelial cells.

Potential toxicity of formulations was addressed measuring the viability of primary human normal fibroblasts (BJ) by MTS cell proliferation assay. BJ cells were preliminary exposed for 6 h to different concentrations (5, 10 and 50 μM) of liposomes **F1a** (DPPC/CHOL), **F2a**, (DPPC/CHOL/SS) **F4a** (DPPC/CHOL/MESO) and their viability was measured at 24 and 48 h after treatment (Fig. 3). Overall, no significant effect on cellular viability was observed under any of the explored experimental conditions. The potential toxicity of **F5a** (DPPC/CHOL/SS/PA-PEG3-mannose) formulation was also evaluated on human primary endothelial cells (HUVEC-Human Umbilical Vein Endothelial Cells). The rationale of evaluating the toxicity of **F5a** formulation on endothelial cells stems from the evidence that these cells express high levels of the GLUT1 transporter protein and should therefore uptake mannose-functionalized **F5a** liposomes with higher efficiency than fibroblasts, possibly resulting in an increased toxicity and reduced viability. However, HUVEC exposed to **F5a** did not show significant cell viability impairment (Supplementary Figure S8).

Then, we addressed the capability of liposomes **F1a**, **F2a**, **F4a** and **F5a** to penetrate cells. We therefore exposed BJ and HUVEC to fluorescent liposomes and addressed by confocal microscopy the presence of labelled liposomes inside the cells. We marked cells by either NBD-PE (green) or rhodamine (red) conjugation for 24 h. We stained cell cytoplasm and cell nucleus by immunoreaction with anti-tubulin antibody and by DAPI, respectively. Confocal analysis of BJ and HUVEC revealed the presence of fluorescent dots in treated cells, confirming the internalization of fluorescent liposomes. Fig. 4 and Supplementary Figure S9 show representative images of BJ and HUVEC cells treated with NBD-PE- and rhodamine-labelled liposomes, respectively.

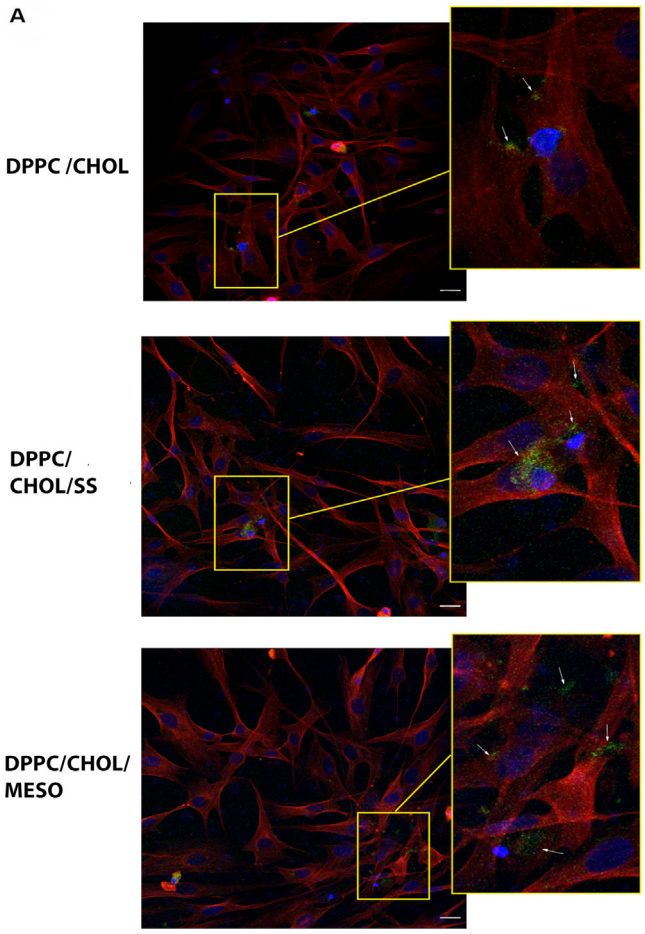

Fig. 4. Confocal microscopy of BJ (A) and HUVEC cells (B) exposed to fluorescent liposomes. The presence of NBD-PE-labelled liposomes (green) is visible at the inner surface of BJ cells (arrows). BJ cytoscheleton was stained by an anti-α tubulin antibody, revealed by an Alexa Fluor 555 secondary antibody (red). Nucleus was stained by DAPI (blue) (A). The presence of rhodamine-labelled liposomes (red) is visible at the inner surface of HUVEC cells (arrows). HUVEC cytoscheleton was stained by an anti-α tubulin antibody, revealed by an Alexa Fluor 488 secondary antibody (green). Nucleus was stained by DAPI (blue) (B). Cell Magnification 40 ×, scale bar 10 μm. (For interpretation of the references to colour in this figure legend, the reader is referred to the web version of this article.)

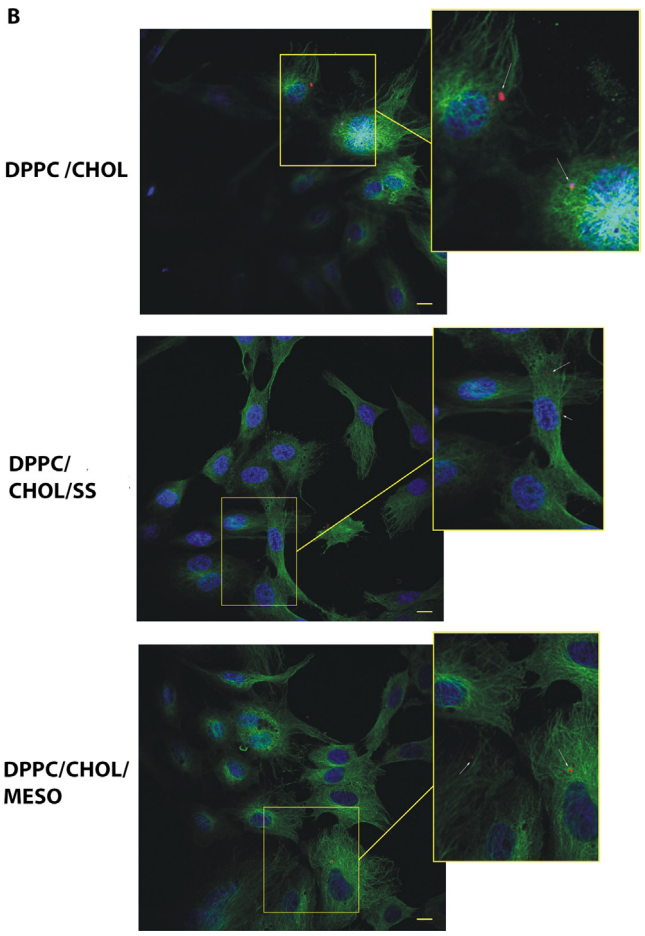

Fig. 4 (*continued*)

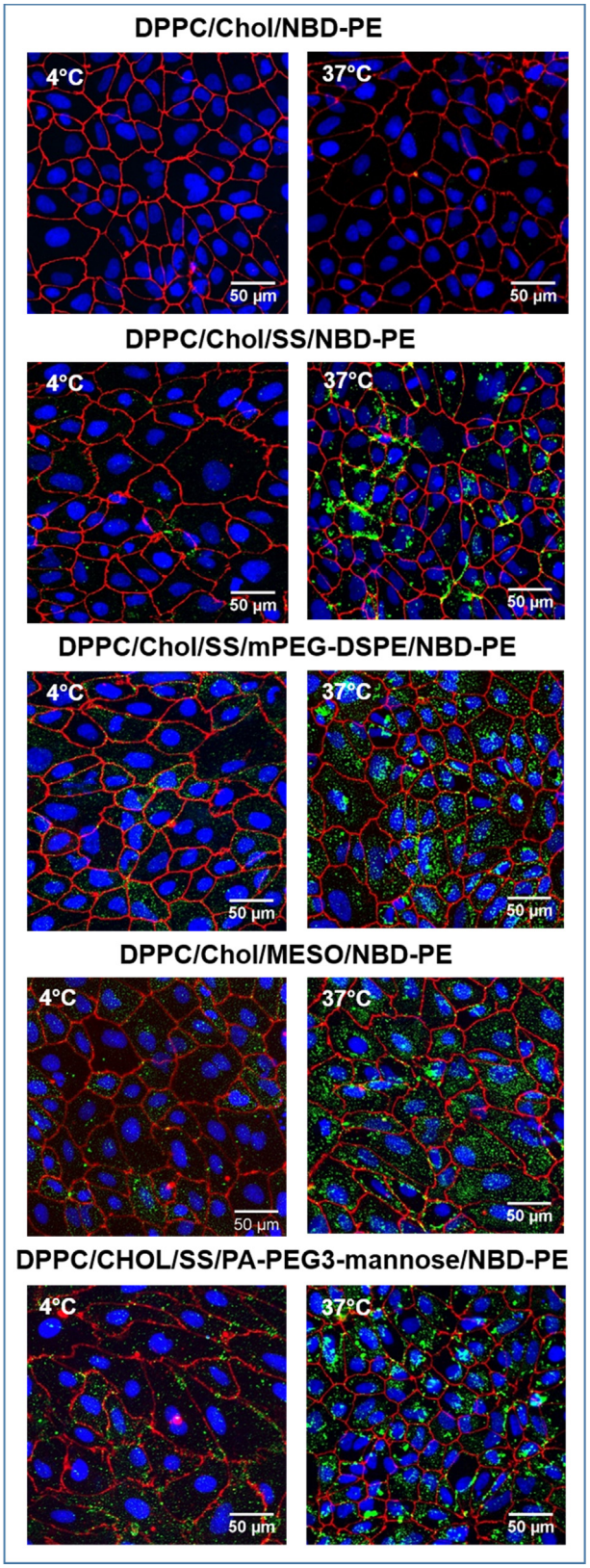

Fig. 5. Uptake of liposomes (NBD-green fluorescence) by cell monolayer. The tight junction protein ZO-1 (red fluorescence) staining showed delineated cell–cell contacts, nuclei were stained in blue (DAPI). Tracking of intracellular distribution by High-content imaging. INCell 6000, Confocal-mode. 20X magnification. (For interpretation of the references to colour in this figure legend, the reader is referred to the web version of this article.)

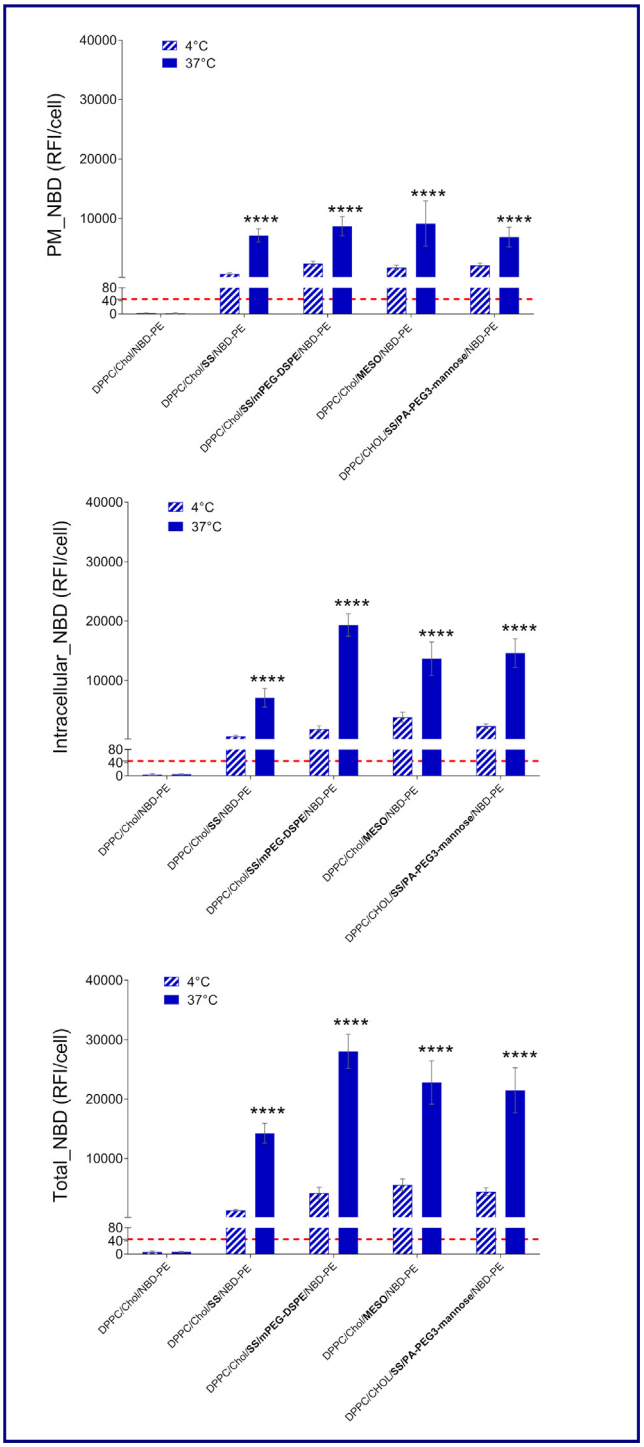

Fig. 6. Quantification of signal associated per cell. The plasma membrane (PM) region was defined through staining of the tight junction protein ZO-1, while the nucleus was identified using DAPI. Images were analyzed via the Developer Toolbox Software. Values presented were means ± SD. LLOQ = 45 RFI/cell (dashed line in red). N = 6 different fields. Statistical analysis: two-way analysis of variance followed by Bonferroni post-test, where ****P < 0.0001, compared to 4 °C incubation group. (For interpretation of the references to colour in this figure legend, the reader is referred to the web version of this article.)

2.3. Haemolytic assays

Experiments on haemolytic activity were performed using the same concentrations as the formulations used for the evaluation

of cytotoxicity against the human fibroblast cell line (5 μM, 10 μM, 50 μM) and adding an additional higher concentration (250 μM). In this way, the total lipid concentration in the test varied from 0.003 mg/mL to 0.15 mg/mL. The results, reported as supplementary material, showed that the formulations had low haemolytic activity (Figure S10) and that the DPPC/CHOL/SS formulation only had haemolytic activity at 250 μM, which is well above the concentration generally considered [72]. Interestingly, the formulation including the SS diastereomer showed different behaviour to the formulation with the MESO diastereomer.

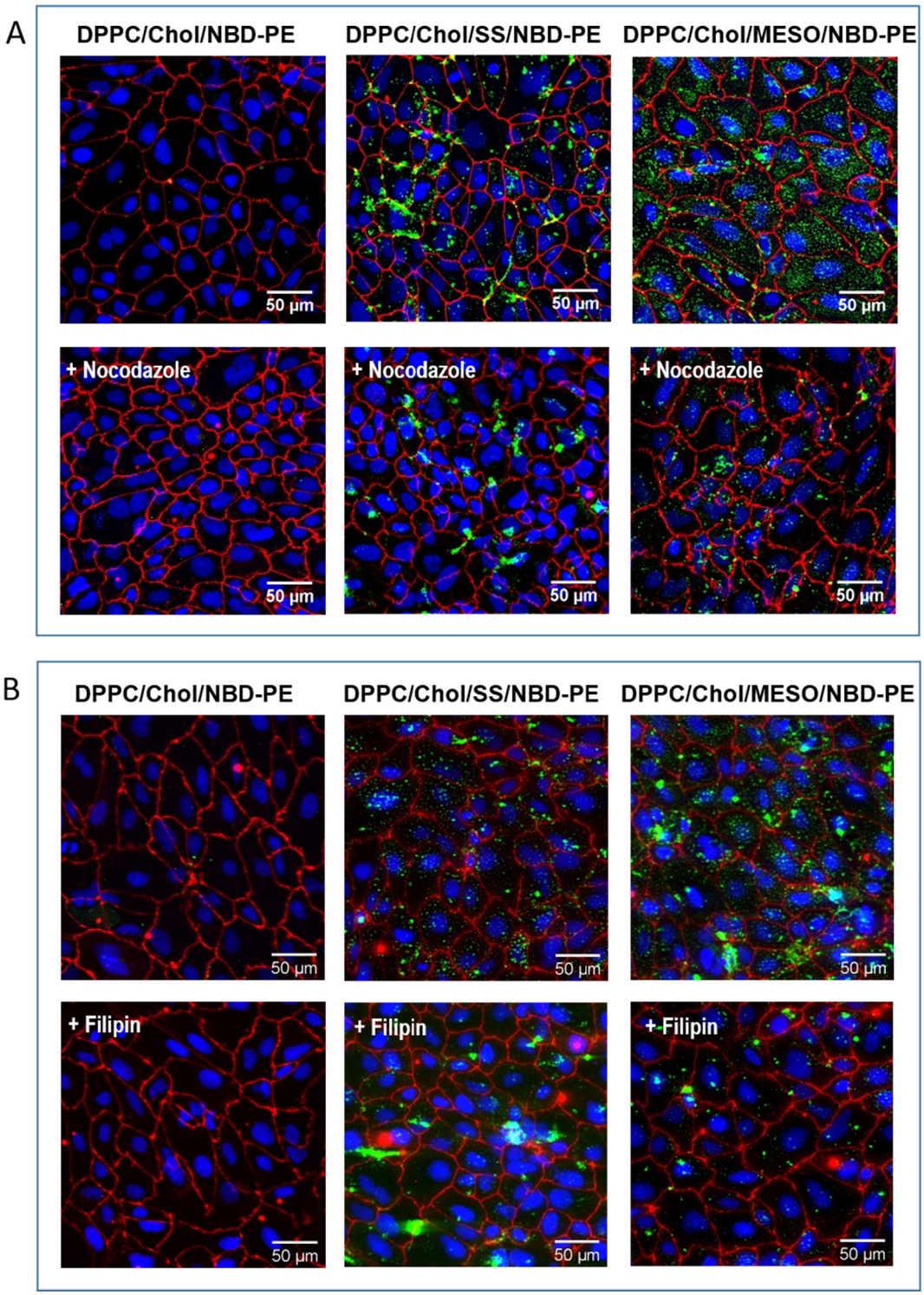

Fig. 7. Uptake of liposomes (NBD-green fluorescence) by cell monolayer in the presence and in the absence of endocytosis inhibitors (nocodazole and filipin). The tight junction protein ZO-1 (red fluorescence) staining showed delineated cell–cell contacts, nuclei were stained in blue (DAPI). Tracking of intracellular distribution by High-content imaging. INCell 6000, Confocal-mode. 20X magnification. (For interpretation of the references to colour in this figure legend, the reader is referred to the web version of this article.)

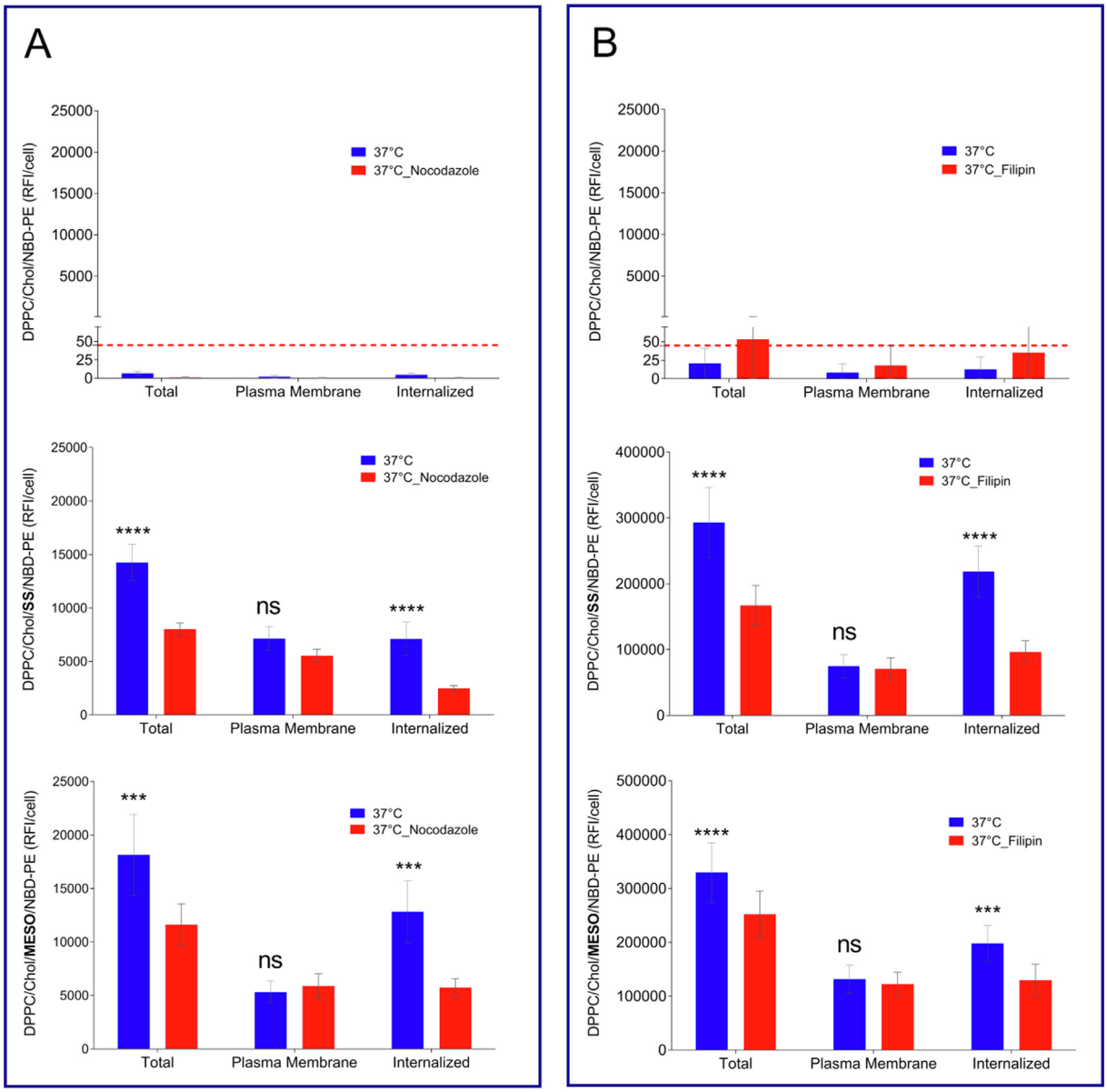

Fig. 8. Quantification of signal associated per cell in the experiments of liposome cell uptake in the presence and in the absence of endocytosis inhibitors (nocodazole and filipin). The plasma membrane (PM) region was defined through staining of the tight junction protein ZO-1, while the nucleus was identified using DAPI. Images were analyzed via the Developer Toolbox Software. Values presented were means ± SD. LLOQ = 45 RFI/cell (dashed line in red). N ≥ 6 different fields. Statistical analysis: two-way analysis of variance followed by Bonferroni post-test, where ****P < 0.0001, ***P < 0.001 or no significant (ns), compared to the incubation in the presence of Nocodazole or Filipin. (For interpretation of the references to colour in this figure legend, the reader is referred to the web version of this article.)

Table 3
Transport of liposomes containing KYNA through the *in vitro* human BBB model compared to the permeability of free KYNA. (Mean ± SEM).

	KYNA Permeability (x10^{-6} cm/*sec*)	Dose transported (%)	TEER (Ω· cm^2)	LY Permeability (x10^{-6} cm/*sec*)
KYNA	1.3 ± 0.4	1.0 ± 0.5	7277 ± 249	0.20 ± 0.03
F1b (DPPC/CHOL)	1.6 ± 0.4	1.3 ± 0.6	3578 ± 394	0.14 ± 0.09
F2b (DPPC/CHOL/SS)	16.2 ± 2.2	13.1 ± 1.8	7080 ± 139	0.26 ± 0.02
F3b (DPPC/CHOL/SS/mPEG-DSPE)	9.9 ± 0.8	8.0 ± 0.6	6348 ± 387	0.56 ± 0.14
F4b (DPPC/CHOL/MESO)	9.8 ± 1.1	7.9 ± 0.9	6301 ± 437	0.57 ± 0.13
F5b (DPPC/CHOL/SS/PA_PEG3-mannose)	<LOQ (0.6)	<LOQ (0.7)	7489 ± 72	0.13 ± 0.04

2.4. Transport of liposomes in iBMECs.

The tropism of liposomes **F1a-F5a** for BCECs was investigated on terminally differentiated iBMECs in monolayer.

Liposomes were labelled with NBD-PE to investigate their internalization. In addition, uptake of the liposomes was carried out at 4 °C and 37 °C and followed for 1 h to assess the existence of active or ATP-driven processes.

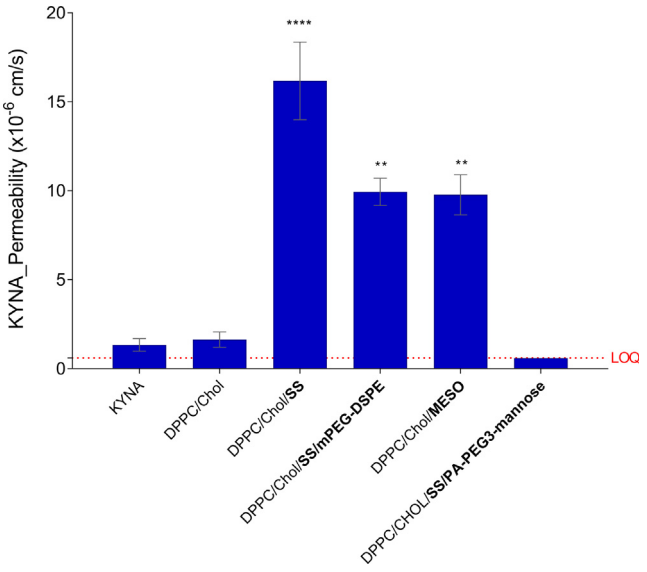

Fig. 9. Permeability of KYNA and liposome-loaded KYNA in the *in vitro* human BBB model. Statistical analysis: one-way analysis of variance followed by Bonferroni post-test, where ****P < 0.0001 and ** P < 0.01 compared to both, KYNA and F1b formulation treatment. LOQ, limit of quantification.

Confocal microscopy observation allowed us to analyse the internalization of NBD labelled liposomes in iBMECs monolayer (Fig. 5) and to quantify the intracellular fluorescence using the InCell Developer Toolbox software (Fig. 6). To visualize the whole cells, the peripheral membrane protein ZO-1 was used as marker. In the case of **F1a** (DPPC/CHOL) liposomes, NBD fluorescence (green) in cells was almost undetectable, thus indicating a very low rate of internalization. On the other hand, the high green fluorescence observed in the case of **F2a**-**F5a** liposomes suggested their internalization by the endothelial cells in monolayer. These results indicated that the presence of gemini amphiphiles in liposome formulation promote internalization. Fluorescent images showed labelled plasma membrane and perinuclear regions, with accumulation of liposomes in the form of droplet structures.

At 4 °C all endocytosis processes were inhibited and transport was less efficient, due to reduced cell-membrane fluidity and dynamics. Internalization levels were lower (2- to 12-folds) compared to 37 °C (Fig. 6), also suggesting the existence of an energy-dependent transport.

Liposomes can be internalized by eukariotic cells using endocytic pathways involving clathrin-mediated endocytosis via coated pits, or endocytic internalization independent of clathrin, such as caveolae-mediated endocytosis. To better investigate the mechanism of entry, internalization of liposomes was investigated by pre-treating the cells with known endocytosis inhibitors for clathrin-mediated endocytosis (nocodazole) or caveolae-mediated endocytosis (filipin). The internalized signal after pre-incubation with nocodazole resulted in significant decrease ($p < 0.0001$ and $p < 0.001$), with a reduction of 65% and 55% uptake for **F2a** (DPPC/CHOL/SS) and **F4a** (DPPC/CHOL/MESO) liposomes, respectively (Fig. 7A and Fig. 8A), which indicated the involvement of clathrin-mediated endocytosis on uptake of liposomes. When the cells were pre-incubated with filipin, the internalized signal significantly decreased ($p < 0.0001$), with a reduction of 56% and 36% uptake for **F2a** (DPPC/CHOL/SS) and **F4a** (DPPC/CHOL/MESO)

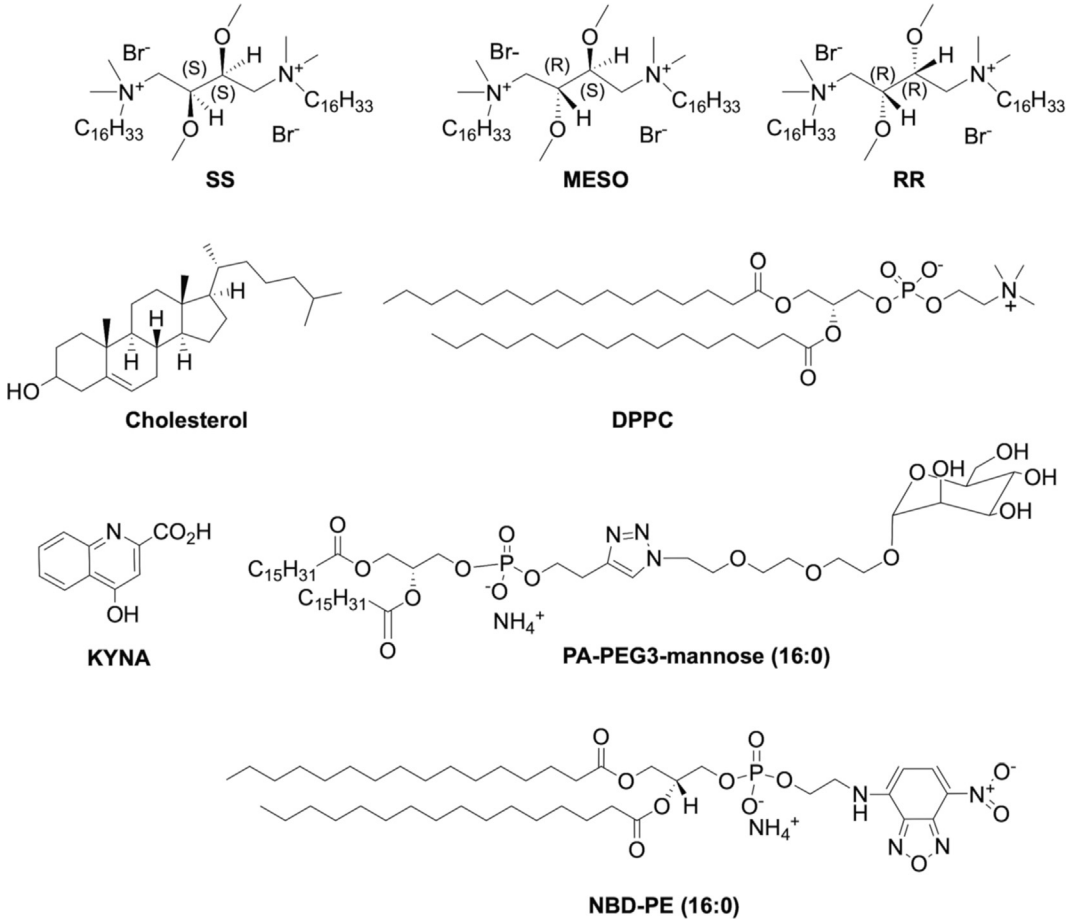

Chart 1. Chart 1. Molecules used for the preparation of liposomes.

liposomes, respectively (Fig. 7B and Fig. 8B). These results suggested that the mechanism of internalizazion of **F2a** and **F4a** involves both clathrin- and caveolae-mediated endocytosis. However, for the liposome formulation **F4a** the prominent endocytotic patway was through clathrin, thus probably involving late endosomes and lysosomes, as previously observed [56].

2.5. Transport studies on an in vitro iBMECs model

The liposomes, previously evaluated in iBMECs monolayer, were loaded with KYNA to assess the passage across the 2D iBMECs transwell model. KYNA is a neuroactive end-product of the kynurenine pathway of tryptophan degradation[73] that was reported to poorly cross the BBB.[74].

The transport of KYNA loaded into liposomes was compared with the permeability of free KYNA (Table 3 and Fig. 9). After 1 h of incubation, samples from the apical (blood side) and basal chamber (brain side) were taken and KYNA was quantified by HPLC. Cells were able to form a functional tight barrier as confirmed by the high TEER (mean 6346 $\Omega{\cdot}cm^2$; threshold$\sim$1000 $\Omega{\cdot}cm^2$) and no significant toxicity was observed. The low permeability of the paracellular marker Lucifer yellow (LY, Permeability < 0.6 × 10–6 cm/s; below the established threshold 1.2–1.3), included as internal control in each filter used for transport studies, indicated the maintenance of the BBB properties for the duration of the whole study. Above a threshold TEER value of 1000 $\Omega{\cdot}cm^2$ the hiPSC-derived BMECs displayed a comparable lucifer yellow permeability, indicating that this TEER values is sufficient to maintain the barrier stability as already demonstrated in our and other laboratory. [43,75,76].

The permeability of KYNA loaded in DPPC/CHOL liposomes (**F1b**) was comparable with that of free KYNA (1.6×10^{-6} cm/s versus 1.3×10^{-6} cm/s, respectively). KYNA entrapped in the liposomes formulated with the gemini amphiphiles (**F2b**-**F4b**) showed instead a significantly higher ($p < 0.01$) permeability with respect to KYNA alone. Moreover, the permeability of KYNA loaded on DPPC/CHOL/SS liposomes (**F2b**) was higher than that of KYNA loaded on DPPC/CHOL/SS/mPEG-DSPE (**F3b**) and on DPPC/CHOL/MESO liposomes (**F4b**).

Crossing of BBB by a molecular species or a nanoparticle involves transcytosis, *i.e.* their internalization of one side of the cell, their transport across the cell and hence the ejection on the other side. As supported by the internalization study, **F3a** and **F4a** as well as **F2a** are internalized in the iBMECs, thus the different permeability across the transport model observed for these formulations suggested that the decoration of liposome surface with PEG or gemini components in the lipid membrane could trigger the activation of additional intracellular pathways that compete with the completion of transcytosis. The different intracellular fate of SS and MESO based liposomes was reported previously, indeed SS containing liposomes were observed mostly in early endosomes whereas MESO containing liposomes were found in late endosomes and lysosomes.[54,56] The permeability of KYNA loaded in **F5b** liposomes (DPPC/CHOL/SS/PA-PEG3-mannose) was under the limit of quantification (200 nM), even though uptake experiments on endothelial cells in monolayer indicated a high extent of cell internalization of **F5a** liposomes. This lack of correlation between transport in brain endothelial cells in monolayer and in the transwell configuration could be due to a difference in the endogenous sorting of the liposomes and to a higher trafficking to the degradation pathway in the BBB model.

3. Conclusion

Cationic liposomes composed of DPPC, cholesterol and a gemini amphiphile (diastereomeric SS or MESO) were formulated and characterized with the aim of investigating their interaction with cell culture models of BBB. The study was focused on the effect of the gemini and their stereochemistry on the capability of liposomes to interact and cross BBB. The effect of the concurrent presence of both a gemini and a mannosylated lipid on liposome features was also studied.

Cell viability assays showed that the investigated liposomes were not toxic at the explored concentrations.

Transport experiments on iBMECs monolayer indicated that the presence of gemini in the formulations promotes internalization in the human brain endothelial cells derived from iPSCs. In addition, their transport across the *in vitro* human BBB model indicated their capability to be first endocytosed and then released at the basolateral side, *i.e.* to be subjected to transcytosis. Indeed, the permeability of KYNA loaded in cationic liposomes containing a gemini amphiphile was significantly higher compared to free KYNA and/or to KYNA loaded in neutral liposomes (DPPC/CHOL), used as controls.

Noteworthy, the capability to cross the BBB model was affected by the stereochemistry of the gemini as the formulation with gemini SS (**F2b**) showed a higher permeability compared to the formulation containing the MESO diastereomer (**F4b**). This result confirms that the stereochemistry of the gemini, by influencing lipid organization and the physico-chemical properties of liposomes, also controls their biological fate. Furthermore, PEG-decorated-liposome (**F3b**) were able to cross the BBB model, though a lower permeability was observed with respect to the non-pegylated formulation **F2b** (9.9 $x10^{-6}$ cm/*sec vs* 16.2 $x10^{-6}$ cm/*sec*, Table 3).

The experiments on liposomes formulated with both gemini SS and a mannosylated lipid surprisingly suggested on the one hand the uptake by iBMECs monolayer but on the other a very low permeability across the BBB model, likely due to a higher trafficking of this formulation to the degradation pathway in the BBB model.

Liposome formulation transport through the BBB seemed to involve more than one mechanism. Firstly, transport of formulations at 4 °C was less efficient due to reduced cell-membrane fluidity and dynamics. Secondly, the treatment of cells with endocytosis-specific inhibitors reduced the uptake of **F2a** and **F4a**. Therefore, liposome formulations use a dynamin-dependent endocytic pathway, including both clathrin- and caveolin-dependent endocytosis.

Probably the involved mechanism is adsorptive-mediated transport, a process triggered at first by electrostatic interactions between the positively charged particle and the negatively charged glycocalyx of BBB endothelial cells, and then mediated by specific interaction between liposomes and cell membrane, as indicated by the differences observed in liposome internalization and transport of KYNA across the BBB. The observed differences can be ascribed to specific interaction of the different liposomes with given lipid domains of cell membrane.

The established *in vitro* iPSC-derived BBB models represent an important advancement in the pre-clinical evaluation of CNS therapeutics towards improving translation.[77] Further studies are needed to describe the extension of the therapeutic potential of these formulations.

4. Experimental material and methods

4.1. Materials and instruments

1,2- dipalmitoyl- *sn*- glycero- 3- phosphocholine (DPPC, >99%); 1,2- distearoyl- *sn*- glycero- 3-phosphoethanolamine-N[methoxy(polyethyleneglycol)2000] (ammonium salt, mPEG-DSPE, >99%); 1,2-dipalmitoyl-*sn*-glycero-3-phospho(ethyl-1′,1′,3′-triazole)trie

thyleneglycolmannose) (ammonium salt, 16:0 PA-PEG3-mannose > 99%); 1-palmitoyl-2-oleoyl-*sn*-glycero-3-phosphocholine (POPC,>99%), 1,2-dipalmitoyl-*sn*-glycero-3-phosphoethanolamine-N-((7-nitro-2–1,3-benzoxadiazol-4-yl) ammonium salt, (NBD-PE 16:0) and 1,2-dipalmitoyl-*sn*-glycero-3-phosphoethanolamine-N-(lissamine rhodamine B sulfonyl) ammonium salt (Rhod-PE 16:0) were purchased from Avanti Polar Lipids (Alabaster, AL, USA). Cholesterol (CHOL, >99%), kynurenic acid (KYNA, >98%) and all reagents and solvents for synthesis were purchased from Aldrich.

Methanol (MeOH), acetonitrile (ACN) and water (HPLC-grade) were purchased from VWR International S.r.l. (Milan, Italy); formic acid was supplied by Carlo Erba (Milan, Italy).

HBSS (Hanks' Balanced Salt solution) buffer solution (pH 7.4) was composed of: 1.26 mM $CaCl_2$, 0.49 mM $MgCl_2{\cdot}6H_2O$, 0.41 mM $MgSO_4{\cdot}7H_2O$, 5.37 mM KCl, 0.44 mM KH_2PO_4, 4.17 mM $NaHCO_3$, 136.9 mM NaCl, 0.34 mM Na_2HPO_4, 5.55 mM Dextrose. HEPES was added to have a final 10 mM concentration.

Gemini amphiphiles SS and MESO were prepared as previously described.[71].

4.2. Preparation and characterization of liposomes

4.2.1. Preparation of empty liposomes

Liposomes were prepared according to the lipid film hydration protocol[78] followed by the extrusion procedure.[79] Proper amounts of lipid and amphiphile solutions (in $CHCl_3$) were poured in a round bottom flask, dried under rotary evaporator and then under high vacuum (6 h) to completely remove the solvent and obtain a thin lipid film. The film was dissolved in HBSS-HEPES buffer solution to get a MLVs suspension of the desired concentration. The suspension was subjected to six freeze–thaw cycles (freezing in liquid nitrogen and heating at 43 °C, *i.e.,* above T_m) and then extruded 10 times (10 mL Lipex Biomembranes extruder) under high pressure through a 100 nm polycarbonate membrane (Whatman Nuclepore) to reduce particle size. In the case of **F3a** (DPPC/CHOL/SS/mPEG-DSPE, Table 1), mPEG-DSPE was added after the extrusion and the resulting solution was left to incubate for 90 min at 60 °C to promote the inclusion of mPEG-DSPE in the lipid bilayer.

Liposomes for monolayer experiments or confocal microscopy investigations were labelled with fluorescent lipids (NBD-PE 16:0, Rhod-PE16:0) that were added to the formulation in the step of lipid film preparation. Fluorescent lipids were 0.3 % of total lipid composition. The presence of the fluorescent lipids did not affect the physico-chemical properties of the liposomes (D_h, PDI, T_m, stability).

4.2.2. Preparation of KYNA-loaded liposomes

Liposomes entrapping KYNA (Table 1) were prepared by the same method described above. In this case, the film was hydrated with a 1 mM KYNA solution (in HBSS–HEPES buffer, pH 7.4) to obtain a 10 mM final concentration of total lipids.

After extrusion, free KYNA was removed from the formulation by size exclusion chromatography following the mini-column centrifugation method [80]: 400 μL of liposome suspension were loaded on a mini-column (1 mL volume) filled with *G-50 sephadex* resin, then the minicolumn was centrifuged at 3000 rpm for 3 min. Free KYNA is retained in the column whereas liposomes are eluted.

4.2.3. Evaluation of KYNA content and release from liposomes

The content of KYNA in liposomes was monitored over a period of 24 h.

From the liposome suspension obtained after the first filtration (corresponding to t_0), portions were taken at different times and filtered on their turn to remove released KYNA.

Each filtered sample was analysed by HPLC to assess residual KYNA into liposomes. The amount of cholesterol was also measured in order to monitor lipid concentration after the filtration and correct KYNA concentration in the various samples in case of dilution due to elution. In the plot (Fig. 2), the percentage of released KYNA is reported as a function of time.

Chromatographic analysis was carried out by a dual Labflow 3000 solvent delivery system (Labservice Analytica Spa, Bologna, Italy) equipped with a Knauer solvent mixing chamber and a model 7125 Rheodyne injector. The system was connected to SPD-M10A diode-array detector supplied by Shimadzu (Milan, Italy). A Synergy 4u Fusion RP-80A, C18 (150 × 4.6 mm id, 4 μm particle size) polar embedded column from Phenomenex (Castel Maggiore, Bologna, Italy), equipped with HPLC guard cartridge system (4 × 3.0 mm) of the same packing material, was employed for the analysis.

Before HPLC analysis, samples were properly diluted with MeOH in order to obtain liposome disruption and complete solubilization of membrane components. Chromatographic elution was carried out in gradient mode by using the following solvent system: 0.1 % formic acid in water (phase A) and 0.1 % formic acid in ACN (phase B). The gradient program was: from 0 to 6 min, 15 % B; from 6 to 10 min, phase B increases up to 100 %, 10–35 min, 100% B. Before use, the mobile phase was degassed for 20 min in an ultrasonic bath. The flow rate was 1 mL min^{-1} and the sample injection volume was 20 μL. KYNA and cholesterol were monitored at 242 nm and 205 nm, respectively.

Method validation was carried out, according to the procedure described above, by assessing linearity, sensitivity and precision. Individual stock standard solutions of KYNA (526 μM) and cholesterol (2000 μM) were prepared in water and in MeOH, respectively. Two different calibration curves were constructed for KYNA by injecting in triplicate working standard solutions in lower (0.5 – 20 μM) and higher (20 – 526 μM) concentration range (n = 6). Both calibration curves were linear in the concentration ranges studied and the correlation coefficients were > 0.9995. In the case of cholesterol, the calibration curve and the linear range of detector response were evaluated by analyzing in triplicate working standard solutions in 25–2000 μM concentration range (n = 6). The linearity was confirmed by R^2 = 0.9998.

Limit of detection (LOD) and limit of quantitation (LOQ) for each analyte were determined by using a signal-to-noise ratio of 3 and 10, respectively. LODs were found to be 60 nM for KYNA and 8 μM for cholesterol. LOQs were found to be 200 nM and 25 μM for KYNA and cholesterol, respectively.

Precision of the method was assessed in terms of repeatability and reproducibility. Intra- and interday precisions, expressed as relative standard deviation (RSD) of migration time and peak area, were evaluated by performing six consecutive injections of the same solution in the same day (RSD < 1 %) and over three days (RSD < 5 %).

4.2.4. Liposome composition

Liposome composition was assessed by NMR, except for KYNA whose concentrations were assessed by HPLC as reported in the previous paragraph. Details are reported in the Supplementary material.

4.2.5. Dynamic light scattering and ζ-potential measurements

Particle size and polydispersity index (PDI) were investigated by dynamic light scattering measurements (DLS). All light scattering measurements were performed by Malvern Nano-ZetaSizer spectrometer equipped with a 5 mW He/Ne laser (λ = 632.8 nm).

This system uses backscatter detection, *i.e.*, the scattered light is collected at an angle of 173°, and this is a significant advantage, because this angle is less sensitive to multiple scattering effects

compared to the more conventional 90°.[81] Temperature was set at 25 °C and the measured autocorrelation function was analysed by using the cumulant fit. The first cumulant was used to obtain the average diffusion coefficients D of the particles further converted into an apparent average hydrodynamic diameter, D_h by using the Stokes–Einstein relationship.

$$D_h = \frac{K_b T}{3\pi\eta \mathrm{D}}$$

where K_bT is the thermal energy and η is the solvent viscosity. The reported values of the hydrodynamic diameter correspond to the average values over several measurements.

All the liposome suspensions were diluted to 1 mM lipid in HBSS–HEPES buffer prior to measurements and samples **F1a**-**F5a** were monitored daily for 14 days to evaluate their stability with regard to aggregation phenomena.

The ζ-potential of cationic formulations was determined from the electrophoretic mobility μ measured using MALVERN NanoZetasizer. Analysis of the Doppler shift to determine the electrophoretic mobility was done by using phase analysis light scattering (PALS)[82], a method that is especially useful at high ionic strengths where mobilities are usually low. The mobility μ was converted into the ζ-potential using the Smoluchowski relation. Liposomes were diluted up to 1 mM in diluted (1:140) HBSS-HEPES buffer and low applied voltages were used to avoid the occurrence of effects due to Joule heating.

4.2.6. T_m determination

The intensity of light scattered at a fixed angle by a liposome solution have been employed to characterize the lipid bilayer organization.[83] It is known that the phase transitions of lipids, at the critical temperature T_m (pre-transition or main transition temperature), implies modifications of lateral diffusion, lateral expansibility, bilayer thickness, bending, permeability, etc., which are reflected in changes of the refractive index. Given the scattered light intensity strictly related to this index the method can be very effective to determine the transition temperature in lipid membranes. The method has been successfully used to determine the thermotropic lipid phase transitions (with characteristic transition temperatures T_m) related to the phase of the lipids in the bilayer [84] and their remodelling within the bilayer.[52].

4.3. In vitro experiments on cellular models

4.3.1. Cell cultures

BJ and HUVEC cells were cultured at 37 °C in a humidified atmosphere containing 5% carbon dioxide. HUVECs (pooled donors) were purchased from ThermoFisher Scientific (Waltham, MA, USA), and grown in complete endothelial cell growth medium (EndoPan 3 Kit, Pan Biotech, Aidenbach, Germany). For the reported experiments, we used HUVECs between passage two and six. BJ were purchased from ATCC (Manassas, VA, USA) and cultured in EMEM (ThermoFisher Scientific), supplemented with 10% fetal bovine serum (ThermoFisher Scientific). Cells were regularly checked to exclude mycoplasma contamination by Mycoalert Detection Kit (Lonza, Basel, Switzerland).

4.3.2. MTS assay

Liposome toxicity was evaluated on both BJ and HUVEC cells viability by Cell Titer 96 Aqueous One Solution Cell Proliferation Assay (Promega, Madison, WI, USA). Two thousand cells were seeded on a 96-well plate in complete medium. Twenty-four hours later, culture medium was replaced by Optimem (ThermoFisher Scientific) and cells exposed to 5, 10 or 50 μM liposomes. After 6 or 24 h exposure, liposomes were removed, and cells cultured in complete growth medium for up to 72 h before MTS. Cell viability was calculated as the ratio between the absorbance of treated and control (sham-treated) cells. Mean values and standard deviation were generated from three biological replicates. Each experiment was performed at least two times.

4.3.3. Confocal microscopy

For detection of fluorescently-labelled liposomes, cells were exposed to 50 μM liposomes for 24 h, washed in PBS and fixed in 4% paraformaldehyde for 15 min. Cytoscheleton was immunostained by primary mouse anti-α-tubulin antibody, 2 h at room temperature (1:250, Sigma-Aldrich, St. Louis, MO, USA). Cells were washed and incubated in PBS containing 5 % Normal Donkey Serum and 1 % BSA with Alexa Fluor 555 or 488 donkey anti-mouse secondary antibody (1:500; Life Technologies, Waltham, MA, USA) for 1 h at RT in humid chamber. Cells were washed, incubated with 4′,6-diamidino-2-phenylindole (DAPI, 1:2000; Sigma-Aldrich, St. Louis, MO, USA) for 5 min, and washed again before mounting the coverslips with mounting medium. Images were acquired using a laser confocal microscope Olympus FV1200, with the following excitation/emission wavelengths: 488/520 nm (green α-tubulin), 553/568 nm (red α-tubulin); 559/591 nm (Rhodamine Red); 463/536 nm (18:1 NBD-PE) and 405/461 nm (DAPI).

4.3.4. Uptake of liposomes on iBMECs

iBMECs differentiated from iPSC, as previously described [43], were plated (2 x10^5 cells/well) on collagen/fibronectin coated 24 well plates (Falcon) and incubated in human endothelial serum-free cell medium (hEC, Thermo Fisher) containing 20 ng/mL bFGF (STEMCELL Tech) and and 1x B27 (Thermo Fisher) with 10 μM retinoic acid (RA, Sigma) for 24 h. After 24 h the medium was changed with hEC without bFGF and RA and incubated for additional 24 h. iBMECs monolayers were then washed twice with HBSS (pH 7.4), containing 10 mM HEPES, and incubated with 500 μL of liposomal formulations for 1 h at both 4 °C and 37 °C. To investigate internalization mechanism, iBMECs were pre-incubated with different endocytosis inhibitors such as nocodazole (35 μM) and filipin (2 μM) for 30 min before application of liposomal formulations.

At the end of incubation, the cells were washed three times with the blocking buffer (phosphate buffered saline (PBS) containing 1% bovine serum albumin (BSA)) to remove unbound or cell-associated liposomes and fixed in 4 % paraformaldehyde for 20 min at room temperature. Cells were permeabilized by washing five times (2 min each) with PBS/0.1 % Triton X-100 and blocked in blocking buffer for 2 h at room temperature. Primary antibodies (anti-ZO1 Mouse Monoclonal antibody, Invitrogen cat.n. 339100), diluted 1:100 in blocking buffer, was added and incubated overnight at 4 °C. Cells were then washed four times and incubated in blocking buffer with the secondary antibody (Rabbit anti-mouse IgG (H + L) Alexa Fluor 594, Life technologies, cat.n. A11062), diluted as recommended by the manufacturer, and the nuclear stain Hoechst 33,342 (2 μM) for one hour at room temperature. At the end of incubation cells were washed three times with phosphate buffered saline (1XPBS) and were imaged with the INCell Analyzer 6000 (GE Healthcare) equipped with a 20X objective lens and a FITC, DAPI, and dsRed excitation/emission filters (488/520, 405/455 and 561/605, respectively). In order to capture enough cells for the analysis (>2000/condition), 6 different fields were acquired/condition. For the quantification analysis, the InCell Developer Toolbox software (GE Healthcare, v1.9) was used. Hoechst 33,342 fluorescence was used to count the number of cells, while ZO1 fluorescence to identify the plasma membrane region of each cell and NBD-PE fluorescence to identify each liposomal spot. Each measure reported as relative fluorescence intensity (RFI) was performed in individual cells and then averaged

within each condition. Cells exposed to NBD-free liposomes were used to calculate the background fluorescence (LLOQ).

4.3.5. Transport experiments

In vitro model of the BBB established by co-culture of iBMECs and human astrocytes[43] was used for transport studies. Measurement of TEER, transport studies and derivation of permeability coefficients were carried out as reported.[85] In each filter, a paracellular marker (Lucifer yellow) was added as internal control of the tightness of the monolayer. Lucifer yellow was quantified by fluorescence spectrophotometry (SAFIRE TECAN, Microplate Fluorescence reader).

4.3.6. Bioanalysis

KYNA was quantitated with the HPLC system previously described in Section 2.1. Aliquots from the receiver and donor chambers were diluted with an equal volume of quenching solution for protein precipitation (0.1% formic acid (FA) in acetonitrile (ACN) containing dextromethorphan (5 μm) as an internal standard (IS). Samples were then vortexed and centrifuged at 4000xg for 10 min at 4 °C. 600 μL of the supernatant were evaporated under nitrogen at 30 °C and reconstituted with 100 μL of mobile phase. In parallel a standard curve was generated and finally, the samples were injected into the HPLC system for analysis. 12 points calibration curve for test compound in duplicate was prepared in HBSS-HEPES buffer and processed as the samples. Procedural blanks were included during analyses to assess the carryover. Limit of quantitation (LOQ) was estimated as the lowest calibration standard concentration, included in the linear range, having a signal-to-noise ratio of 10. It was found to be 31.3 nM. The proper mobile phases and gradient conditions were selected to obtain the best retention and separation of the test compound. Mobile phase consisted of water (phase A) and ACN (phase B), both acidified with 0.1% formic acid. In particular, the elution profile was as follow: 0–6 min, 85–15% B (v/v); 6–17 min, 15–50% B; 17–18 min, 50% B; 18–19 min, 50–100 %B; 19–37 min, 100% B. KYNA and IS were monitored at 242 nm and 280 nm, respectively.

4.3.7. Statistical analysis

Statistical analysis was performed using one-way (liposome-loaded KYNA) or two-way (NBD-PE labelled liposomes) analysis of variance (ANOVA) followed by Bonferroni multiple comparison post-hoc test (GraphPad Prism 8.4.3, San Diego, CA, USA). Formulations were tested in triplicate, at least two independent experiments were performed, and data are expressed as mean ± standard deviation (SD) or standard error of the mean (SEM). The difference was considered statistically significant for $P < 0.05$.

5. Supplementary material

Determination of final liposome composition by NMR, confocal microscopy images and haemolytic assays are available as supplementary material.

Conflict of interest.

The authors declare no competing financial interests.

CRediT authorship contribution statement

Beatrice Simonis: Investigation, Data curation, Formal analysis, Writing – original draft. **Domenico Vignone:** Investigation, Data curation, Formal analysis. **Odalys Gonzalez Paz:** Conceptualization, Methodology, Validation, Data curation, Writing – original draft. **Enrica Donati:** Methodology, Investigation, Validation, Data curation, Writing – original draft. **Maria Laura Falchetti:** Methodology, Investigation, Validation, Writing – review & editing, Funding acquisition. **Cecilia Bombelli:** Conceptualization, Methodology, Writing – review & editing. **Antonella Cellucci:** Investigation, Visualization. **Giulio Auciello:** Investigation, Visualization. **Ivan Fini:** Investigation, Visualization. **Luciano Galantini:** Methodology, Validation, Formal analysis, Funding acquisition. **Rudaba Zaman Syeda:** Investigation, Visualization. **Marco Mazzonna:** Investigation, Validation, Data curation. **Maria Patrizia Mongiardi:** Investigation, Data curation, Writing – original draft. **Francesco Buonocore:** Investigation, Data curation, Formal analysis. **Francesca Ceccacci:** Conceptualization, Methodology, Validation, Funding acquisition, Writing – original draft, Writing – review & editing, Supervision. **Annalise Di Marco:** Conceptualization, Methodology, Validation, Writing – review & editing, Funding acquisition, Supervision. **Giovanna Mancini:** Conceptualization, Methodology, Writing – review & editing, Funding acquisition, Supervision.

Declaration of Competing Interest

The authors declare that they have no known competing financial interests or personal relationships that could have appeared to influence the work reported in this paper.

Acknowledgments

B.S. is grateful to Regione Lazio project “Torno Subito” Ed. 2018, for financial support.

This work was supported by Regione Lazio -through the project “Lipobarr” (Progetti Gruppi di Ricerca- Conoscenza e Cooperazione per un Nuovo Modello di Sviluppo- PROT. N. 85-2017-15057) and by Ministero dell’Università e della Ricerca through the project “CNCCS-Centre for rare, neglected and poverty related diseases”.

We thank Dr. Valentina Ricci for helpful assistance in confocal microscopy.

Appendix A. Supplementary data

Supplementary data to this article can be found online at https://doi.org/10.1016/j.jcis.2022.07.025.

References

[1] W.M. Pardridge, Drug transport across the blood-brain barrier, J. Cereb. Blood Flow Metab. 32 (2012) 1959–1972, https://doi.org/10.1038/jcbfm.2012.126.
[2] A. Gaudin, O. Tagit, D. Sobot, S. Lepetre-Mouelhi, J. Mougin, T.F. Martens, K. Braeckmans, V. Nicolas, D. Desmaële, S.C. de Smedt, N. Hildebrandt, P. Couvreur, K. Andrieux, Transport mechanisms of squalenoyl-adenosine nanoparticles across the blood-brain barrier, Chem. Mater. 27 (2015) 3636–3647, https://doi.org/10.1021/acs.chemmater.5b00267.
[3] S. Ding, A.I. Khan, X. Cai, Y. Song, Z. Lyu, D. Du, P. Dutta, Y. Lin, Overcoming blood-brain barrier transport: Advances in nanoparticle-based drug delivery strategies, Mater. Today 37 (2020) 112–125, https://doi.org/10.1016/j.mattod.2020.02.001.
[4] W.M. Pardridge, Blood-brain barrier delivery, Drug Discovery Today 12 (2007) 54–61, https://doi.org/10.1016/j.drudis.2006.10.013.
[5] A.G. de Boer, P.J. Gaillard, Drug targeting to the brain, Annu. Rev. Pharmacol. Toxicol. 47 (2007) 323–355, https://doi.org/10.1146/annurev.pharmtox.47.120505.105237.
[6] N.J. Abbott, Blood-brain barrier structure and function and the challenges for CNS drug delivery, J. Inherit. Metab. Dis. 36 (2013) 437–449, https://doi.org/10.1007/s10545-013-9608-0.
[7] D. Furtado, M. Björnmalm, S. Ayton, A.I. Bush, K. Kempe, F. Caruso, Overcoming the Blood-Brain Barrier: The Role of Nanomaterials in Treating Neurological Diseases, Adv. Mater. 30 (46) (2018) 1801362.
[8] J. Saint-Pol, F. Gosselet, S. Duban-Deweer, G. Pottiez, Y. Karamanos, Targeting and Crossing the Blood-Brain Barrier with Extracellular Vesicles, Cells. 9 (4) (2020) 851.
[9] A. Amit, S. Sabahuddin, A. Mukta, Ajazuddin, M.S. Ahmed, A.S. Mahmoud, A.U. R. Syed, I.M.A. Mohi, A.S. Mohamed, Nanotechnology: A non-invasive diagnosis and therapeutic tool for brain disorders, African J. Pharmacy Pharmacology. 13 (10) (2019) 118–123.

[10] A. Jain, S.K. Jain, In vitro release kinetics model fitting of liposomes: An insight, Chem. Phys. Lipids 201 (2016) 28–40, https://doi.org/10.1016/J.CHEMPHYSLIP.2016.10.005.
[11] Z. Drulis-Kawa, A. Dorotkiewicz-Jach, Liposomes as delivery systems for antibiotics, Int. J. Pharm. 387 (2010) 187–198, https://doi.org/10.1016/J.IJPHARM.2009.11.033.
[12] T.M. Allen, P.R. Cullis, Liposomal drug delivery systems: From concept to clinical applications, Adv. Drug Deliv. Rev. 65 (2013) 36–48, https://doi.org/10.1016/J.ADDR.2012.09.037.
[13] E. Moghimipour, A. Salimi, Liposomes as a Novel Drug Delivery System: Fundamental and Pharmaceutical Application, Asian, J. Pharmaceutics. 12 (2018) 31–41, https://doi.org/10.22377/ajp.v12i01.2037.
[14] M. Li, C. Du, N. Guo, Y. Teng, X. Meng, H. Sun, S. Li, P. Yu, H. Galons, Composition design and medical application of liposomes, Eur. J. Med. Chem. 164 (2019) 640–653, https://doi.org/10.1016/J.EJMECH.2019.01.007.
[15] I.Y. Wu, S. Bala, N. Škalko-Basnet, M.P. di Cagno, Interpreting non-linear drug diffusion data: Utilizing Korsmeyer-Peppas model to study drug release from liposomes, Eur. J. Pharm. Sci. 138 (2019), https://doi.org/10.1016/J.EJPS.2019.105026 105026.
[16] B. Sheikholeslami, N.W. Lam, K. Dua, M. Haghi, Exploring the impact of physicochemical properties of liposomal formulations on their in vivo fate, Life Sci. 300 (2022), https://doi.org/10.1016/j.lfs.2022.120574 120574.
[17] L. Sercombe, T. Veerati, F. Moheimani, S.Y. Wu, A.K. Sood, S. Hua, Advances and challenges of liposome assisted drug delivery, Front. Pharmacol. 6 (2015), https://doi.org/10.3389/fphar.2015.00286.
[18] A.D. Bangham, R.W. Horne, Negative staining of phospholipids and their structural modification by surface-active agents as observed in the electron microscope, J. Mol. Biol. 8 (5) (1964) 660–IN10.
[19] J. Song, C. Lu, J. Leszek, J. Zhang, Design and development of nanomaterial-based drug carriers to overcome the blood–brain barrier by using different transport mechanisms, Int. J. Mol. Sci. 22 (18) (2021) 10118.
[20] G. Sharma, A.R. Sharma, S.S. Lee, M. Bhattacharya, J.S. Nam, C. Chakraborty, Advances in nanocarriers enabled brain targeted drug delivery across blood brain barrier, Int. J. Pharm. 559 (2019) 360–372, https://doi.org/10.1016/j.ijpharm.2019.01.056.
[21] J. Ahlawat, G. Guillama Barroso, S. Masoudi Asil, M. Alvarado, I. Armendariz, J. Bernal, X. Carabaza, S. Chavez, P. Cruz, V. Escalante, S. Estorga, D. Fernandez, C. Lozano, M. Marrufo, N. Ahmad, S. Negrete, K. Olvera, X. Parada, B. Portillo, A. Ramirez, R. Ramos, V. Rodriguez, P. Rojas, J. Romero, D. Suarez, G. Urueta, S. Viel, M. Narayan, Nanocarriers as Potential Drug Delivery Candidates for Overcoming the Blood-Brain Barrier: Challenges and Possibilities, ACS, Omega. 5 (22) (2020) 12583–12595.
[22] F. Juhairiyah, E.C.M. de Lange, Understanding Drug Delivery to the Brain Using Liposome-Based Strategies: Studies that Provide Mechanistic Insights Are Essential, AAPS J. 23 (2021), https://doi.org/10.1208/s12248-021-00648-z.
[23] R. Alyautdin, I. Khalin, M.I. Nafeeza, M.H. Haron, D. Kuznetsov, Nanoscale drug delivery systems and the blood-brain barrier, Int. J. Nanomed. 9 (2014) 795–811, https://doi.org/10.2147/IJN.S52236.
[24] M.I. Teixeira, C.M. Lopes, M.H. Amaral, P.C. Costa, Current insights on lipid nanocarrier-assisted drug delivery in the treatment of neurodegenerative diseases, Eur. J. Pharm. Biopharm. 149 (2020) 192–217, https://doi.org/10.1016/j.ejpb.2020.01.005.
[25] A. Lindqvist, J. Rip, J. van Kregten, P.J. Gaillard, M. Hammarlund-Udenaes, In vivo Functional Evaluation of Increased Brain Delivery of the Opioid Peptide DAMGO by Glutathione-PEGylated Liposomes, Pharm. Res. 33 (2016) 177–185, https://doi.org/10.1007/s11095-015-1774-3.
[26] J.M. Lajoie, E. v. Shusta, Targeting receptor-mediated transport for delivery of biologics across the blood-brain barrier, Annu. Rev. Pharmacol. Toxicol. 55 (2015) 613–631, https://doi.org/10.1146/annurev-pharmtox-010814-124852.
[27] E.M. McConnell, M.R. Holahan, M.C. Derosa, Aptamers as promising molecular recognition elements for diagnostics and therapeutics in the central nervous system, Nucleic Acid Ther. 24 (2014) 388–404, https://doi.org/10.1089/nat.2014.0492.
[28] V.M. Pulgar, Transcytosis to cross the blood brain barrier, new advancements and challenges, Front. Neurosci. 13 (2019), https://doi.org/10.3389/fnins.2018.01019.
[29] Q. Lu, X. Cai, X. Zhang, S. Li, Y. Song, D. Du, P. Dutta, Y. Lin, Synthetic Polymer Nanoparticles Functionalized with Different Ligands for Receptor-Mediated Transcytosis across the Blood-Brain Barrier, ACS Applied Bio Materials. 1 (2018) 1687–1694, https://doi.org/10.1021/acsabm.8b00502.
[30] D.J. Lundy, H. Nguy n, P.C.H. Hsieh, Emerging nano-carrier strategies for brain tumor drug delivery and considerations for clinical translation, Pharmaceutics. 13 (8) (2021) 1193.
[31] J. Kreuter, Drug delivery to the central nervous system by polymeric nanoparticles: What do we know?, Adv Drug Deliv. Rev. 71 (2014) 2–14, https://doi.org/10.1016/j.addr.2013.08.008.
[32] Y.C. Kuo, C.Y. Lin, Targeting delivery of liposomes with conjugated p-aminophenyl-α-D-manno-pyranoside and apolipoprotein E for inhibiting neuronal degeneration insulted with β-amyloid peptide, J. Drug Target. 23 (2015) 147–158, https://doi.org/10.3109/1061186X.2014.965716.
[33] Z.F. Hao, Y.X. Cui, M.H. Li, D. Du, M.F. Liu, H.Q. Tao, S. Li, F.Y. Cao, Y.L. Chen, X.H. Lei, L. Wang, D.L. Zhu, H.S. Peng, C.L. Jiang, Liposomes modified with P-aminophenyl-α-d-mannopyranoside: A carrier for targeting cerebral functional regions in mice, Eur. J. Pharm. Biopharm. 84 (2013) 505–516, https://doi.org/10.1016/J.EJPB.2012.12.020.
[34] P.P. Karmali, A. Chaudhuri, Cationic liposomes as non-viral carriers of gene medicines: Resolved issues, open questions, and future promises, Med. Res. Rev. 27 (2007) 696–722, https://doi.org/10.1002/med.20090.
[35] C.R. Dass, P.F.M. Choong, Targeting of small molecule anticancer drugs to the tumour and its vasculature using cationic liposomes: Lessons from gene therapy, Cancer Cell International. 6 (2006), https://doi.org/10.1186/1475-2867-6-17.
[36] W. Chen, H. Li, Z. Liu, W. Yuan, Lipopolyplex for therapeutic gene delivery and its application for the treatment of Parkinson's disease, Front. Aging Neurosci. 8 (2016), https://doi.org/10.3389/fnagi.2016.00068.
[37] C. Bombelli, F. Faggioli, P. Luciani, G. Mancini, M.G. Sacco, Efficient transfection of DNA by liposomes formulated with cationic gemini amphiphiles, J. Med. Chem. 48 (2005) 5378–5382, https://doi.org/10.1021/jm050477r.
[38] B. dos Santos Rodrigues, H. Oue, A. Banerjee, T. Kanekiyo, J. Singh, Dual functionalized liposome-mediated gene delivery across triple co-culture blood brain barrier model and specific in vivo neuronal transfection, Journal of Controlled Release. 286 (2018) 264–278. https://doi.org/10.1016/j.jconrel.2018.07.043.
[39] X.B. Zhao, N. Muthusamy, J.C. Byrd, R.J. Lee, Cholesterol as a bilayer anchor for PEGylation and targeting ligand in folate-receptor-targeted liposomes, J. Pharm. Sci. 96 (2007) 2424–2435, https://doi.org/10.1002/jps.20885.
[40] W.A. Banks, S.M. Robinson, A. Nath, Permeability of the blood–brain barrier to HIV-1 Tat, Exp. Neurol. 193 (2005) 218–227, https://doi.org/10.1016/J.EXPNEUROL.2004.11.019.
[41] M. Strazza, V. Pirrone, B. Wigdahl, M.R. Nonnemacher, Breaking down the barrier: The effects of HIV-1 on the blood–brain barrier, Brain Res. 1399 (2011) 96–115, https://doi.org/10.1016/J.BRAINRES.2011.05.015.
[42] M. Toborek, Y.W. Lee, G. Flora, H. Pu, I.E. András, E. Wylegala, B. Hennig, A. Nath, Mechanisms of the blood-brain barrier disruption in HIV-1 infection, Cell. Mol. Neurobiol. 25 (2005) 181–199, https://doi.org/10.1007/s10571-004-1383-x.
[43] A. Di Marco, D. Vignone, O. Gonzalez Paz, I. Fini, M.R. Battista, A. Cellucci, E. Bracacel, G. Auciello, M. Veneziano, V. Khetarpal, M. Rose, A. Rosa, I. Gloaguen, E. Monteagudo, T. Herbst, C. Dominguez, I. Muñoz-Sanjuán, Establishment of an in Vitro Human Blood-Brain Barrier Model Derived from Induced Pluripotent Stem Cells and Comparison to a Porcine Cell-Based System, Cells. 9 (4) (2020) 994.
[44] C. Bombelli, G. Caracciolo, P. di Profio, M. Diociaiuti, P. Luciani, G. Mancini, C. Mazzuca, M. Marra, A. Molinari, D. Monti, L. Toccacieli, M. Venanzi, Inclusion of a photosensitizer in liposomes formed by DMPC/gemini surfactant: Correlation between physicochemical and biological features of the complexes, J. Med. Chem. 48 (2005) 4882–4891, https://doi.org/10.1021/jm050182d.
[45] A. Molinari, M. Colone, A. Calcabrini, A. Stringaro, L. Toccacieli, G. Arancia, S. Mannino, A. Mangiola, G. Maira, C. Bombelli, G. Mancini, Cationic liposomes, loaded with m-THPC, in photodynamic therapy for malignant glioma, Toxicol. In Vitro 21 (2007) 230–234, https://doi.org/10.1016/j.tiv.2006.09.006.
[46] A. Molinari, C. Bombelli, S. Mannino, A. Stringaro, L. Toccacieli, A. Calcabrini, M. Colone, A. Mangiola, G. Maira, P. Luciani, G. Mancini, G. Arancia, m-THPC-mediated photodynamic therapy of malignant gliomas: Assessment of a new transfection strategy, Int. J. Cancer 121 (2007) 1149–1155, https://doi.org/10.1002/ijc.22793.
[47] C. Bombelli, S. Borocci, M. Diociaiuti, F. Faggioli, L. Galantini, P. Luciani, G. Mancini, M.G. Sacco, Role of the Spacer of Cationic Gemini Amphiphiles in the Condensation of, DNA (2005), https://doi.org/10.1021/la051324.
[48] V. Perri, M. Pellegrino, F. Ceccacci, A. Scipioni, S. Petrini, E. Gianchecchi, A. Lo Russo, S. De Santis, G. Mancini, A. Fierabracci, P. Heneberg, Use of short interfering RNA delivered by cationic liposomes to enable efficient down-regulation of PTPN22 gene in human T lymphocytes, PLoS ONE 12 (4) (2017) e0175784.
[49] M. Pellegrino, F. Ceccacci, S. Petrini, A. Scipioni, S. de Santis, M. Cappa, G. Mancini, A. Fierabracci, Exploiting novel tailored immunotherapies of type 1 diabetes: Short interfering RNA delivered by cationic liposomes enables efficient down-regulation of variant PTPN22 gene in T lymphocytes, Nanomedicine: Nanotechnology, Biology Medicine. 18 (2019) 371–379, https://doi.org/10.1016/J.NANO.2018.11.001.
[50] A. Arena, E. Belcastro, F. Ceccacci, S. Petrini, L.A. Conti, O. Pagliarosi, E. Giorda, S. Sennato, R. Schiaffini, P. Wang, J.C. Paulson, G. Mancini, A. Fierabracci, Improvement of Lipoplexes With a Sialic Acid Mimetic to Target the C1858T PTPN22 Variant for Immunotherapy in Endocrine Autoimmunity, Front. Immunol. 13 (2022), https://doi.org/10.3389/fimmu.2022.838331.
[51] S. Aleandri, C. Bombelli, M.G. Bonicelli, F. Bordi, L. Giansanti, G. Mancini, M. Ierino, S. Sennato, Fusion of gemini based cationic liposomes with cell membrane models: Implications for their biological activity, Biochimica et Biophysica Acta - Biomembranes. 2013 (1828) 382–390, https://doi.org/10.1016/j.bbamem.2012.10.001.
[52] D.A. Jaeger, E. Kubicz-Loring, R.C. Price, H. Nakagawa, Vesicular Properties of Stereoisomeric Surfactants, Vesicular Properties of Stereoisomeric Surfactants 12 (24) (1996) 5803–5808.
[53] C. Bombelli, A. Stringaro, S. Borocci, G. Bozzuto, M. Colone, L. Giansanti, R. Sgambato, L. Toccaceli, G. Mancini, A. Molinari, Efficiency of liposomes in the delivery of a photosensitizer controlled by the stereochemistry of a gemini surfactant component, Mol. Pharm. 7 (2010) 130–137, https://doi.org/10.1021/mp900173v.
[54] S. Aleandri, M.G. Bonicelli, F. Bordi, S. Casciardi, M. Diociaiuti, L. Giansanti, F. Leonelli, G. Mancini, G. Perrone, S. Sennato, How stereochemistry affects the

physicochemical features of gemini surfactant based cationic liposomes, Soft Matter 8 (2012) 5904–5915, https://doi.org/10.1039/c2sm25193k.
[55] E. Stefanutti, F. Papacci, S. Sennato, C. Bombelli, I. Viola, A. Bonincontro, F. Bordi, G. Mancini, G. Gigli, G. Risuleo, Cationic liposomes formulated with DMPC and a gemini surfactant traverse the cell membrane without causing a significant bio-damage, Biochimica et Biophysica Acta (BBA) -, Biomembranes. 1838 (10) (2014) 2646–2655.
[56] S. Borocci, G. Bozzuto, C. Bombelli, F. Ceccacci, G. Formisano, A. Stringaro, A. Molinari, G. Mancini, How stereochemistry of lipid components can affect lipid organization and the route of liposome internalization into cells, Nanoscale. 13 (2021) 11976–11993, https://doi.org/10.1039/d1nr02175c.
[57] L. Xu, X. Wang, W. Wang, M. Sun, W.J. Choi, J.Y. Kim, C. Hao, S. Li, A. Qu, M. Lu, X. Wu, F.M. Colombari, W.R. Gomes, A.L. Blanco, A.F. de Moura, X. Guo, H. Kuang, N.A. Kotov, C. Xu, Enantiomer-dependent immunological response to chiral nanoparticles, Nature 601 (2022) 366–373, https://doi.org/10.1038/s41586-021-04243-2.
[58] G. Bozzuto, A. Molinari, Liposomes as nanomedical devices, Int. J. Nanomed. 10 (2015) 975–999, https://doi.org/10.2147/IJN.S68861.
[59] D. Lombardo, P. Calandra, D. Barreca, S. Magazù, M. Kiselev, Soft interaction in liposome nanocarriers for therapeutic drug delivery, Nanomaterials. 6 (7) (2016) 125.
[60] J.M. Harris, Introduction to biotechnical and biomedical applications of poly (ethylene glycol), Springer, New York, 1992.
[61] K. Hristova, A. Kenworthy, T.J. Mcintosh11, Effect of Bilayer Composition on the Phase Behavior of Liposomal Suspensions Containing Poly(ethylene glycol)-Lipids, (1995). https://pubs.acs.org/sharingguidelines.
[62] A.K. Kenworthy, K. Hristova, D. Needham, T.J. McIntosh, Range and magnitude of the steric pressure between bilayers containing phospholipids with covalently attached poly(ethylene glycol), Biophys. J . 68 (5) (1995) 1921–1936.
[63] A.K. Kenworthy, S.A. Simon, T.J. McIntosh, Structure and phase behavior of lipid suspensions containing phospholipids with covalently attached poly (ethylene glycol), Biophys. J . 68 (5) (1995) 1903–1920.
[64] D. Hanahan, R.A. Weinberg, The Hallmarks of Cancer, Cell 100 (2000) 57–70, https://doi.org/10.1016/S0092-8674(00)81683-9.
[65] N. Dos Santos, C. Allen, A.-M. Doppen, M. Anantha, K.A.K. Cox, R.C. Gallagher, G. Karlsson, K. Edwards, G. Kenner, L. Samuels, M.S. Webb, M.B. Bally, Influence of poly(ethylene glycol) grafting density and polymer length on liposomes: Relating plasma circulation lifetimes to protein binding, Biochimica et Biophysica Acta (BBA) -, Biomembranes. 1768 (6) (2007) 1367–1377.
[66] J. Heyes, K. Hall, V. Tailor, R. Lenz, I. MacLachlan, Synthesis and characterization of novel poly(ethylene glycol)-lipid conjugates suitable for use in drug delivery, J. Control. Release 112 (2006) 280–290, https://doi.org/10.1016/J.JCONREL.2006.02.012.
[67] A.L. Klibanovl, K. Maruyamal, V.P. Torchilin2, L. Huangl, Amphipathic polyethyleneglycols effectively prolong the circulation time of liposomes, (1990).
[68] M.C. Woodle, D.D. Lasic, Sterically stabilized liposomes, Sterically stabilized liposomes 1113 (2) (1992) 171–199.
[69] J.-H. Fuhrhop, W. Helfrich, Fluid and Solid Fibers Made of Lipid Molecular Bilayers, (1985). https://pubs.acs.org/sharingguidelines.
[70] K. Morigaki, S. Dallavalle, P. Walde, S. Colonna, P.L. Luisi, Autopoietic Self-Reproduction of Chiral Fatty Acid Vesicles, (1997). https://pubs.acs.org/sharingguidelines.
[71] C. Bello, C. Bombelli, S. Borocci, P. di Profio, G. Mancini, Role of the spacer stereochemistry on the aggregation properties of cationic gemini surfactants, Langmuir 22 (2006) 9333–9338, https://doi.org/10.1021/la061230f.
[72] S. Mourtas, G.P.A.K. Michanetzis, Y.F. Missirlis, S.G. Antimisiaris, Haemolytic activity of liposomes: Effect of vesicle size, lipid concentration and polyethylene glycol-lipid or arsonolipid incorporation, J. Biomed. Nanotechnol. 5 (2009) 409–415, https://doi.org/10.1166/jbn.2009.1050.
[73] R. Schwarcz, J.P. Bruno, P.J. Muchowski, H.Q. Wu, Kynurenines in the mammalian brain: When physiology meets pathology, Nat. Rev. Neurosci. 13 (2012) 465–477, https://doi.org/10.1038/nrn3257.
[74] S. Fukui, R. Schwarcz, S.I. Rapoport, Y. Takada, Q.R. Smith, Blood-Brain Barrier Transport of Kynurenines, Implications for Brain Synthesis and Metabolism 56 (6) (1991) 2007–2017.
[75] E.H. Neal, N.A. Marinelli, Y. Shi, P.M. McClatchey, K.M. Balotin, D.R. Gullett, K.A. Hagerla, A.B. Bowman, K.C. Ess, J.P. Wikswo, E.S. Lippmann, A. Simplified, Fully Defined Differentiation Scheme for Producing Blood-Brain Barrier Endothelial Cells from Human iPSCs, Stem Cell Rep. 12 (2019) 1380–1388, https://doi.org/10.1016/j.stemcr.2019.05.008.
[76] J.L. Mantle, L. Min, K.H. Lee, Minimum Transendothelial Electrical Resistance Thresholds for the Study of Small and Large Molecule Drug Transport in a Human in Vitro Blood-Brain Barrier Model, Mol. Pharm. 13 (2016) 4191–4198, https://doi.org/10.1021/acs.molpharmaceut.6b00818.
[77] M. Ribecco-Lutkiewicz, C. Sodja, J. Haukenfrers, A.S. Haqqani, D. Ly, P. Zachar, E. Baumann, M. Ball, J. Huang, M. Rukhlova, M. Martina, Q. Liu, D. Stanimirovic, A. Jezierski, M. Bani-Yaghoub, A novel human induced pluripotent stem cell blood-brain barrier model: Applicability to study antibody-triggered receptor-mediated transcytosis, Sci. Rep. 8 (2018), https://doi.org/10.1038/s41598-018-19522-8.
[78] R.C.; M.R.I. MacDonald, Liposome Technology 2nd Ed, 2nd ed., CRC Press, Bosca Raton Florida, (1992).
[79] M.J.; N.R.; M.L.D.; C.P.R. Hope, Liposome Technology 2nd, 2nd Ed, CRC Press, Bosca Raton Florida, (1992).
[80] D.W. Fry, J.C. White, I. David Goldman', Rapid Separation of Low Molecular Weight Solutes from Liposomes without Dilution, (1978).
[81] H.S. Dhadwal, R.R. Ansari, W.V. Meyer, A fiber-optic probe for particle sizing in concentrated suspensions, Rev. Sci. Instrum. 62 (1991) 2963–2968, https://doi.org/10.1063/1.1142190.
[82] W.W. Tscharnuter, Mobility measurements by phase analysis, Appl. Opt. 40 (2001) 3995–4003.
[83] B.J.P.R. Berne, Dynamic light scattering: with applications to chemistry, biology and physics, Biomedical Education, John Wiley & Sons, New York, 1976.
[84] N. Michel, A.S. Fabiano, A. Polidori, R. Jack, B. Pucci, Determination of phase transition temperatures of lipids by light scattering, Chem. Phys. Lipids 139 (2006) 11–19, https://doi.org/10.1016/J.CHEMPHYSLIP.2005.09.003.
[85] A. di Marco, O. Gonzalez Paz, I. Fini, D. Vignone, A. Cellucci, M.R. Battista, G. Auciello, L. Orsatti, M. Zini, E. Monteagudo, V. Khetarpal, M. Rose, C. Dominguez, T. Herbst, L. Toledo-Sherman, V. Summa, I. Munoz-Sanjuán, Application of an in Vitro Blood-Brain Barrier Model in the Selection of Experimental Drug Candidates for the Treatment of Huntington's Disease, Molecular Pharmaceutics. 16 (2019) 2069–2082. https://doi.org/10.1021/acs.molpharmaceut.9b00042.